Structure and dynamics of the SARS-CoV -2 envelope protein monomer

Alexander Kuzmin, Philipp Orekhov, Roman Astashkin, Valentin Gordeliy, Ivan Gushchin

Structure and dynamics of the SARS-CoV-2 envelope protein monomer

Alexander Kuzmin[1] | Philipp Orekhov[1,2,3] | Roman Astashkin[1,4] | Valentin Gordeliy[1,4,5,6] | Ivan Gushchin[1]

[1]Research Center for Molecular Mechanisms of Aging and Age-related Diseases, Moscow Institute of Physics and Technology, Dolgoprudny, Russia

[2]Faculty of Biology, M.V. Lomonosov Moscow State University, Moscow, Russia

[3]Faculty of Biology, Shenzhen MSU-BIT University, Shenzhen, China

[4]Institut de Biologie Structurale (IBS), Université Grenoble Alpes, CEA, CNRS, Grenoble, France

[5]Institute of Biological Information Processing (IBI-7: Structural Biochemistry), Forschungszentrum Jülich GmbH, Jülich, Germany

[6]JuStruct: Jülich Center for Structural Biology, Forschungszentrum Jülich GmbH, Jülich, Germany

Correspondence
Ivan Gushchin, Research Center for Molecular Mechanisms of Aging and Age-related Diseases, Moscow Institute of Physics and Technology, Dolgoprudny, Russia.
Email: ivan.gushchin@phystech.edu

Funding information
Commissariat à l'Energie Atomique et aux Energies Alternatives; Helmholtz-Gemeinschaft Deutscher Forschungszentren; Ministry of Science and Higher Education of the Russian Federation

Abstract

Coronaviruses, especially severe acute respiratory syndrome coronavirus 2 (SARS-CoV-2), present an ongoing threat to human wellbeing. Consequently, elucidation of molecular determinants of their function and interaction with the host is an important task. Whereas some of the coronaviral proteins are extensively characterized, others remain understudied. Here, we use molecular dynamics simulations to analyze the structure and dynamics of the SARS-CoV-2 envelope (E) protein (a viroporin) in the monomeric form. The protein consists of the hydrophobic α-helical transmembrane domain (TMD) and amphiphilic α-helices H2 and H3, connected by flexible linkers. We show that TMD has a preferable orientation in the membrane, while H2 and H3 reside at the membrane surface. Orientation of H2 is strongly influenced by palmitoylation of cysteines Cys40, Cys43, and Cys44. Glycosylation of Asn66 affects the orientation of H3. We also observe that the monomeric E protein both generates and senses the membrane curvature, preferably localizing with the C-terminus at the convex regions of the membrane; the protein in the pentameric form displays these properties as well. Localization to curved regions may be favorable for assembly of the E protein oligomers, whereas induction of curvature may facilitate the budding of the viral particles. The presented results may be helpful for a better understanding of the function of the coronaviral E protein and viroporins in general, and for overcoming the ongoing SARS-CoV-2 pandemic.

KEYWORDS
envelope protein, glycosylation, membrane curvature, membrane protein, molecular dynamics, palmitoylation, SARS-CoV-2

1 | INTRODUCTION

Coronaviruses (CoVs) (order *Nidovirales*, family *Coronaviridae*, subfamily *Coronavirinae*) are enveloped viruses with a positive-sense, single-stranded RNA genome of ~30 kb, one of the largest among RNA viruses.[1] CoVs infect birds and mammals, causing a variety of fatal diseases. They can also infect humans and cause diseases ranging from the common cold to acute respiratory distress syndrome. Highly pathogenic human coronaviruses include Severe Acute Respiratory Syndrome Coronavirus (SARS)-CoV, Middle Eastern Respiratory SyndromeCoronavirus (MERS)-CoV, and severe acute respiratory syndrome coronavirus 2 (SARS-CoV-2).[2,3] The outbreaks of SARS-CoV in 2002/3 and MERS-CoV in 2012 led to epidemics. SARS-CoV-2 emerged at the end of December 2019 causing a pandemic of the coronavirus disease 2019 (COVID-19), which is a novel life-threatening form of atypical pneumonia.[4]

Antiviral strategies may be roughly divided into two classes: the measures aimed at prevention of the spread of infections, and treatment of patients who have already contracted the disease. The development of both kinds of strategies benefits greatly from understanding the virus physiology, and in particular the structure and function of viral proteins. Structural biology studies of SARS-CoV-2 have seen rapid progress since the beginning of the pandemic.[5] Whereas most of the key information was obtained using experimental techniques, such as cryo-electron microscopy, x-ray crystallography, or nuclear magnetic resonance (NMR), computational approaches were key for some of the findings.[6,7] Among the most notable examples are detailed simulations of dynamics of the most important viral proteins[6,8,9] or even the whole virion,[10] early generation of atomic models for all SARS-CoV-2 proteins,[11] and high-throughput virtual ligand screening of viral protease inhibitors.[12,13]

The genomes of all coronaviruses encode four major structural proteins: the spike (S) protein, the nucleocapsid (N) protein, the membrane (M) protein, and the envelope (E) protein.[14] The S protein is involved in host recognition, attachment, and cell fusion. The N protein is involved in the packaging of the RNA genome and the formation of the nucleocapsid. The M protein directs the assembly process of virions through interactions with the other structural proteins and defines the shape of the viral envelope. The E protein is possibly the most mysterious of them since it is associated with the assembly of virions, effective virion transfer along the secretory pathway as well as a reduced stress response by the host cell. Generally, it promotes virus fitness and pathogenesis.[15]

Overall, coronaviral E proteins are small, integral membrane proteins of 75–109 amino acids, which have at least one helical transmembrane domain (TMD) and a long amphiphilic region comprising one or two α-helices at the C-terminus.[16,17] SARS-CoV-2 E protein consists of 75 amino acids, and its sequence is 95% and 36% identical to those of SARS-CoV and MERS-CoV E proteins, respectively. Given the sequence identity and the available data, SARS-CoV and SARS-CoV-2 E proteins appear to be very similar in their structure and function, and most of the findings about the former proteins likely apply to the latter as well. The general properties of the SARS-CoV-2 E protein presumably match those of other coronaviral E proteins.

It was shown previously that E proteins may undergo co-translational and/or posttranslational modifications (CPTMs),[16,17] but the role of these modifications is still not fully clear. The prominent examples of other viral proteins that may be also modified by palmitoylation are the coronaviral S protein, haemagglutinin (HA) protein of the influenza virus, Env proteins of retroviruses and filoviruses, and vaccinia virus 37 kDa major envelope antigen (p37).[18–21] Some results indicate that conserved cysteines of the SARS-CoV E protein and, presumably, their palmitoylation are functionally important for the stability of the E protein and the overall virus production.[22,23] On the other hand, glycosylation shields viral proteins from recognition by the immune system.[24,25] It is closely linked to the protein topology as modification can happen only in the lumen of endoplasmic reticulum. SARS-CoV and SARS-CoV-2 E proteins are predominantly inserted in the membrane with their C-termini in the cytoplasm and are not modified[23,26–28]; a minor fraction can be glycosylated under certain non-native conditions.[23,27] The role of this possible glycosylation of E proteins is not clear.[17]

Only a small fraction of the E protein expressed during infection is incorporated into the virion envelope; the rest is localized at the intracellular trafficking endoplasmic reticulum (ER)-Golgi region and mostly at the intermediate compartment between ER and ER-Golgi intermediate compartment (ERGIC).[22,26,29–32] ERGIC is composed of tubulovesicular membrane clusters, with many curved membrane regions.[33] CoVs assemble and bud at the ERGIC, where the E protein may induce membrane curvature or aid in membrane scission.[16,17] Indeed, various recombinant CoVs lacking the gene for E exhibit an aberrant morphology, from which it can be concluded that the function of E is to induce membrane curvature of the viral envelope, thus allowing CoV particles to acquire their characteristic spherical shape and morphology.[30,34,35] E protein was also shown to colocalize and interact with the M and N proteins[36,37] as well as with the N-terminus of nsp3.[38] It increases the expression of the M and S proteins[39] and, together with M, affects the processing, maturation, and localization of S.[29] Finally, it can also interact with cellular proteins Bcl-xL,[40] PALS1,[41,42] and others such as CWC27, AP3B1, ZC3H18, SLC44A2, BRD2, and BRD4.[43]

In the host membranes, E proteins oligomerize to form ion-conductive pores[44–47] that may be inhibited by hexamethylene amiloride (HMA) and amantadine.[48–52] Similar small proteins (60–120 residues), which oligomerize and form hydrophilic transmembrane pores or channels and disrupt a number of physiological characteristics of the cell, are called viroporins.[53] They are known to contribute to the release of infectious enveloped virus particles from infected cells and/or to facilitate the penetration of the viruses into the cell. The most famous representative viroporins of highly pathogenic RNA viruses are human immunodeficiency virus type 1 (HIV-1) Viral protein U (Vpu) protein, hepatitis C virus p7 protein, and influenza A virus matrix protein 2 (M2), which are involved in diverse processes such as virus entry, trafficking, assembly, inflammation, and apoptosis.[53] The significant contribution of viroporins to the life cycle of viruses makes them a target for therapeutic interventions. In particular, M2 can be targeted by FDA-approved inhibitor rimantadine.[54] Investigations have shown that SARS-CoV viruses, in which the channel activity is inhibited, were much less infectious and pathogenic.[55]

Currently, several experimental structures of the E protein fragments are available.[46,49,51,56,57] In particular, it was shown that the protein contains a TM (transmembrane) α-helix and one (when in monomeric form and in detergent[56]) or two (when in pentameric form[57]), amphipathic α-helices. Yet, the experimental structure of the full-length wild-type protein is not available at the moment, and the influence of CPTMs on it has not been studied. Moreover, there is little data on the behavior of monomeric E protein prior to its assembly into pentameric channels. In the present study, we applied molecular dynamics simulations to study the behavior of monomeric E protein from SARS-CoV-2 and identified the effects of CPTMs on the protein behavior. We have also observed that the protein induces curvature in the membranes, and is attracted to the curved regions. These findings may be helpful in development of anti-SARS-CoV-2 medications, and for understanding the function of viroporins in general.

2 | RESULTS

2.1 | Structure of the monomeric E protein

E protein from SARS-CoV-2 is a 75 amino acid-long protein that may be palmitoylated and glycosylated in vivo (Figure 1A). To assess the overall conformational space available to the protein, we conducted first an extensive coarse-grained (CG) simulation of unmodified E protein, followed by atomistic simulations of unmodified protein and CG simulations of the protein with modifications (Table S1). CG simulations are known to faithfully reproduce the major physicochemical properties of the studied macromolecules while providing a considerable speedup compared to atomistic simulations.[58,59]

In accordance with expectations, the simulations revealed that the protein is very flexible with no particular tertiary structure (Figure 1B). Principal component analysis (PCA) shows that the first two components describe most of the structural variation (∼64%, Figure 2) and correspond to motions of the helices H2 and H3 relative to each other and TMD near the membrane surface.

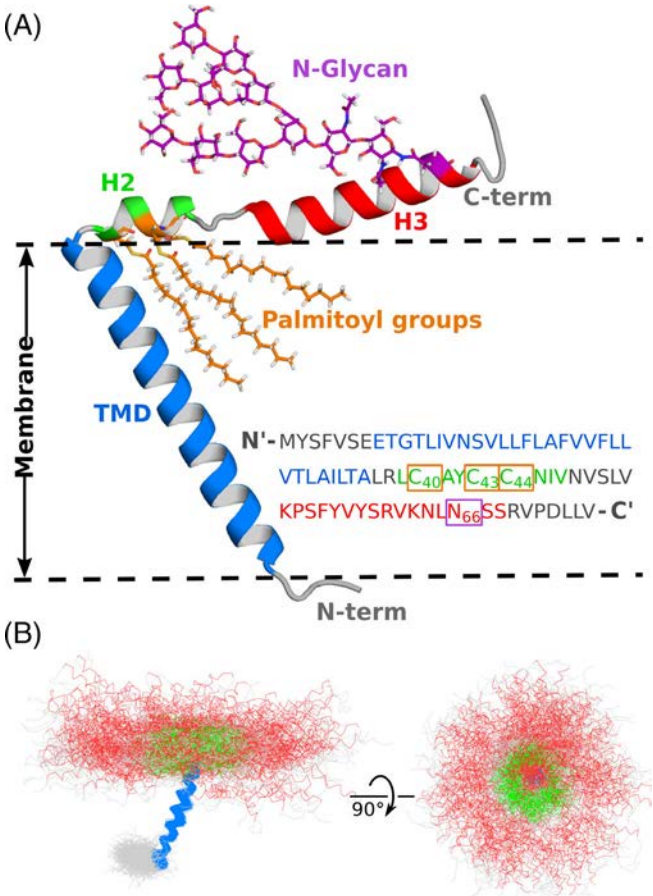

FIGURE 1 Structure of the SARS-CoV-2 envelope (E) protein monomer with possible co- and post-translational modifications. (A) Schematic model showing a fully palmitoylated and glycosylated E protein. Transmembrane domain is shown in blue and amphipathic helices H2 and H3 are shown in green and red. (B) Conformations of the unmodified E protein observed in coarse-grained simulations. Positions of the transmembrane helix were aligned for clarity; helices H2 and H3 are mobile

Atomistic simulations are considerably more computationally demanding, and thus the exhaustive sampling of the conformational space can take a prohibitively long time. Consequently, we simulated a number of atomistic trajectories starting from representative conformations from the CG simulation. We divided the CG trajectory snapshots into four clusters and used the centroids of the clusters as the starting structures for atomistic simulations. For each starting structure, we obtained six trajectories of the E protein: three with the protein embedded in the model membrane containing POPC, and three with the membrane mimicking the natural ERGIC membrane (50% POPC, 25% POPE, 10% POPI, 5% POPS, and 10% cholesterol). No qualitative differences were observed between the simulations conducted in these membranes. Overall, PCA shows that the atomistic simulations correspond to the CG simulation and display roughly the same conformational space available to the E protein (Figure 2B). Conformations observed in atomistic simulations are shown in Figure S1.

Atomistic simulations also show that while the secondary structure of the E protein is largely conserved, the amphipathic α-helices H2 and H3 may partially unfold, with H2 being more disordered (Figures 3 and S2). We observed both unfolding and refolding events. Overall, this observation is in agreement with NMR experiments.[56,57]

2.2 | Position of the E protein elements relative to the membrane

Figure 4 shows the average positions of the secondary structure elements of the E protein relative to the membrane surface. In all of the simulations, the TMD remained embedded in the membrane. H2 is deeply buried in the lipid headgroup region, whereas H3 is slightly removed from the membrane border, while still remaining in contact with it. In some atomistic trajectories, partial unbinding of H3 from the membrane is observed (Figure S3).

Interestingly, TMD, despite being a single transmembrane α-helix, has a preferable orientation in the membrane (Figures 5 and S4). It is tilted at the angle of 25°–40° in all of the simulations and has a strong orientational (azimuthal) preference, with phenylalanines Phe20, Phe23, and Phe26 oriented toward the N-terminal side. No robust effects of CPTMs modifications on the orientation of TMD were observed (Table S2).

H2, as an amphipathic helix, also has a preferred orientation (Figures 6 and S5). Its three cysteines, Cys40, Cys43, and Cys44, may be palmitoylated in vivo, which would change the physicochemical properties of the helix. To probe the effects of all possible combinations of these PTMs in an efficient manner, we employed CG simulations. We found that palmitoylation, on average, leads to the rotation of H2 around its axis (Figure 6, Table S2). The strongest effect on the H2 orientation is observed when Cys40 and Cys44 are palmitoylated simultaneously: the helix is rotated by ∼32.2° relative to its position in the unmodified protein. Other palmitoylated variants have intermediate orientations; the effects of palmitoylation of the three cysteine residues are not additive (Table S2). Finally, whereas the position of H3 was not significantly affected by palmitoylation, it was affected by glycosylation (Supporting Text and Figure S6).

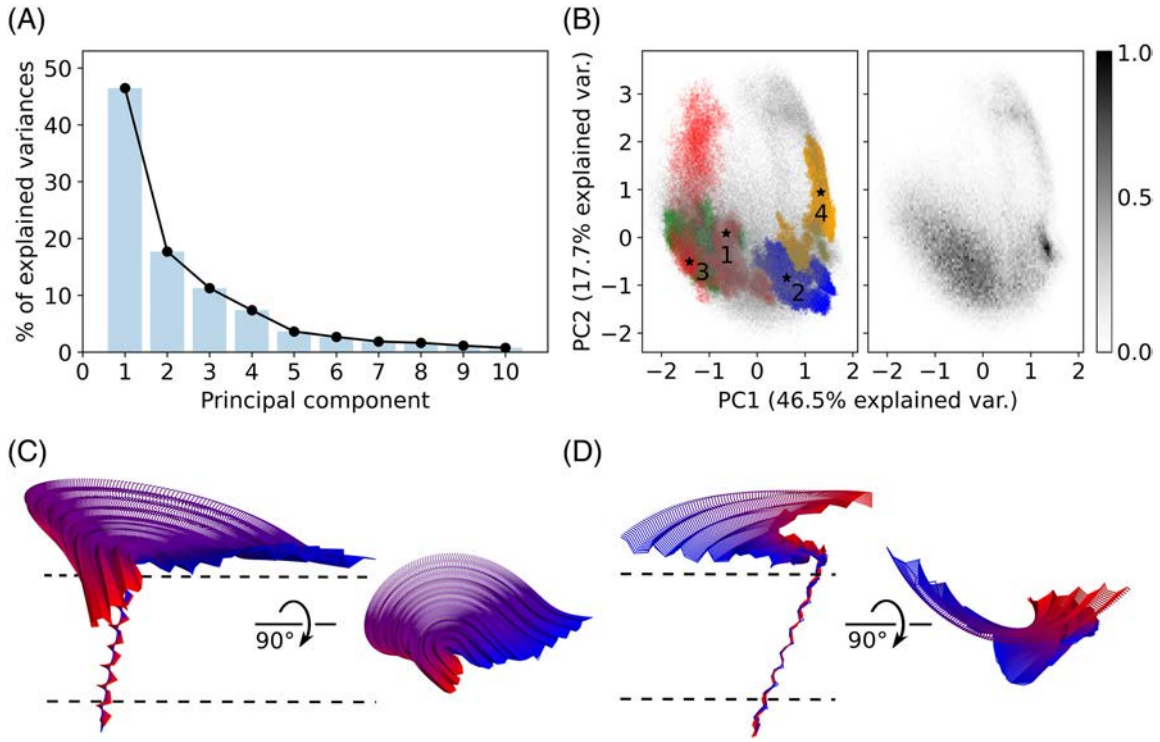

FIGURE 2 Comparison of the E protein conformations observed in atomistic (AA) and coarse-grained (CG) simulations using principal component analysis (PCA). (A) The scree plot for the top 10 PCA eigenvalues. First two components describe ~64% of structural variations. (B) Comparison of the conformational ensembles observed in AA (colored) and CG (gray) simulations projected onto PC1 and PC2. The data for CG simulations only are shown on the right. Starting conformations for AA simulations are labeled with stars. Trajectories from the first, second, third, and fourth sets of AA simulations are shown in red, blue, green, and orange, respectively. (C) Conformational changes associated with PC1. (D) Conformational changes associated with PC2. The structures are colored from blue to red according to the PC projection value. Approximate membrane position is shown with the dashed lines

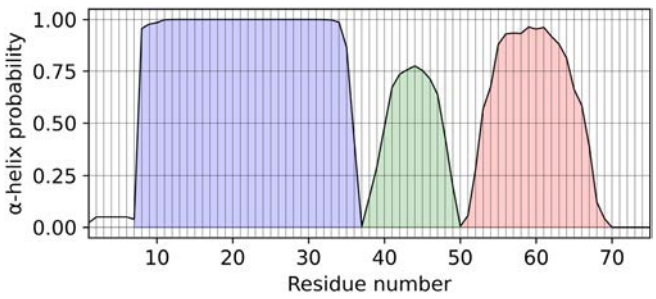

FIGURE 3 Conservation of the secondary structure of the E protein in AA MD simulations. Average probability of observing the α-helical structure for each residue is shown. TMD remains fully α-helical, whereas H2 and H3 can be sometimes disordered (H2 is disordered more often compared to H3)

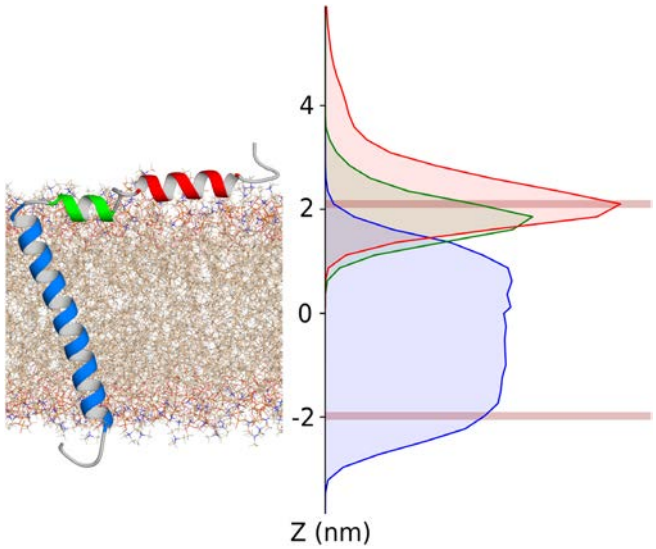

FIGURE 4 Average positions of TMD, H2, and H3 relative to the membrane in all atom simulations. Average positions of lipid phosphate groups are shown using brown lines. Distributions of TMD, H2, and H3 backbone atoms' positions are shown in blue, green, and red, respectively

2.3 | Induction of curvature by the E protein

In all of the conducted simulations, we observed induction of curvature by the E protein: the membrane bends toward the side where the C-terminus is located in both CG (Figure 7A) and atomistic (Figure S8) simulations. The effect is also observed in larger systems containing

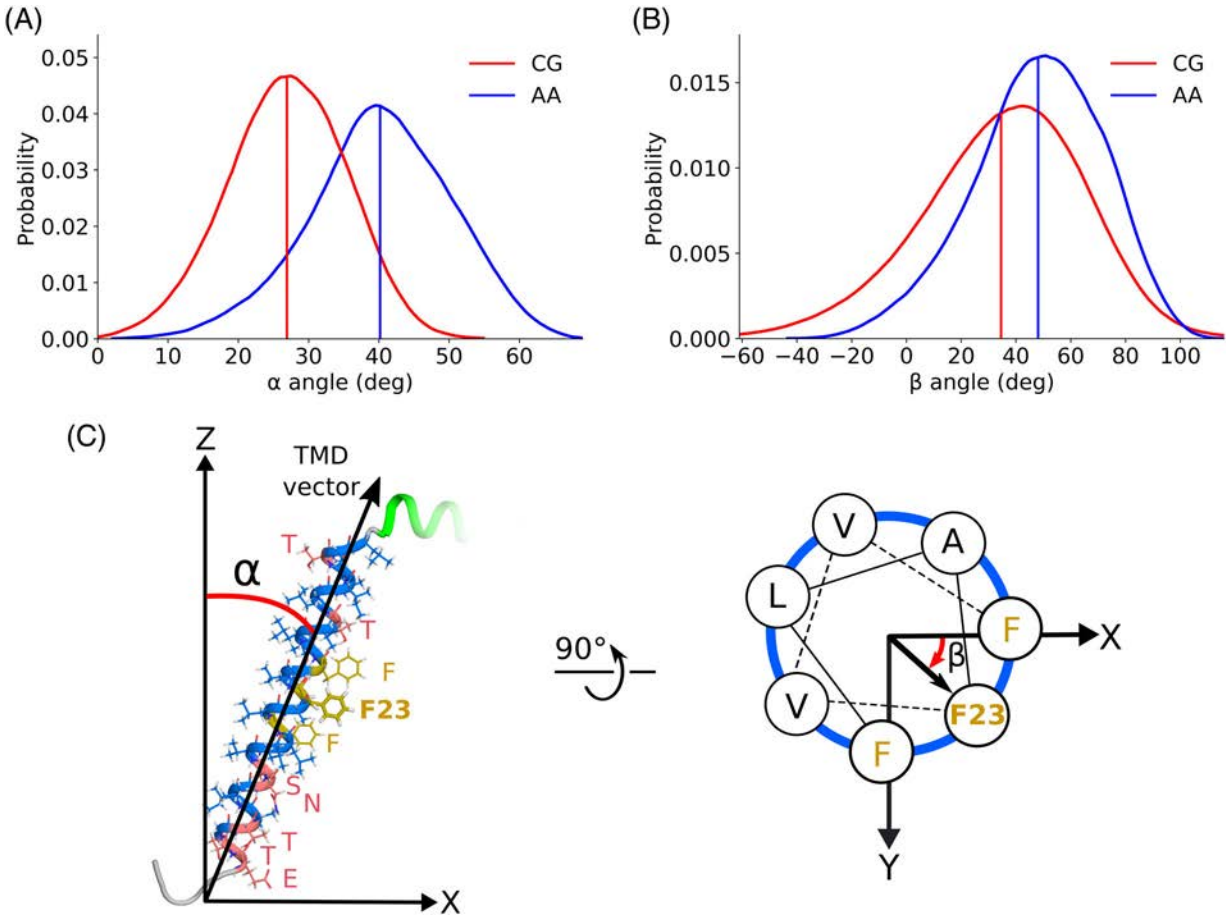

FIGURE 5 Orientation of TMD in POPC bilayer in coarse-grained (CG) and all atom (AA) simulations. (A) Distributions of the tilt angles. (B) Distributions of the axial rotation angles. Vertical lines indicate average values. (C) Definitions of the tilt (α) and axial rotation (β) angles

four E protein monomers in opposite orientations (Figure S7). Presumably, the curvature is induced by the amphipathic helices that embed into the adjacent leaflet and expand it.

To check whether the curvature is indeed induced by H2 and H3, we conducted additional CG simulations of artificial proteins consisting of only TMD or only H2 and H3 (Figure 7B,C). Isolated TMD was tilted in a way similar to that observed in the simulations of the full-length protein. The membrane was perturbed and thinned near the α-helix (Figure 7B), presumably because of the polar residues on the respective sides (Glu8, Thr9, Thr11, Asn15, Ser16 at the N-terminal side, Thr30, Thr35 at the C-terminal side). Isolated H2 and H3 curved the membrane in the same way as the full-length protein (Figure 7C). Thus, we conclude that the structural elements responsible for curvature induction by the E protein are the amphipathic helices of the C-terminal domain.

2.4 | Dynamics of the E protein within curved membranes

Having observed the induction of curvature by the E protein, we were also interested to check whether it has a preferable position in membranes that are already curved, such as the native ER, Golgi, and ERGIC membranes, especially during the budding of virus-like particles (VLPs). As a test system, we used artificially buckled membranes.[60–63] Given the size of the systems (Table S1), the simulations were conducted in CG representation. Irrespective of the starting positions, E protein monomers redistribute in the membranes so that the C-termini localize to the convex regions (Figure 8). The effect was observed both in the membranes buckled in a single direction (nonzero mean curvature, zero Gaussian curvature, Figure 8A) and in the membranes buckled in both directions (nonzero Gaussian curvature, Figure 8B). Thus, we conclude that the monomeric E protein is curvature-sensitive.

2.5 | Properties of the pentameric E protein

To see whether the pentameric E protein can also generate and/or sense curvature, we conducted additional CG simulations (Figure 9). Using the computational model by Heo and Feig[11] or the more recent NMR model[51] (for TMD) as a starting structure, we obtained similar conformational ensembles. The C-terminal helices do not have a fixed position (Figure 9A). Both H2 and H3 are slightly removed from the membrane in simulations of the pentameric E protein (Figure S9)

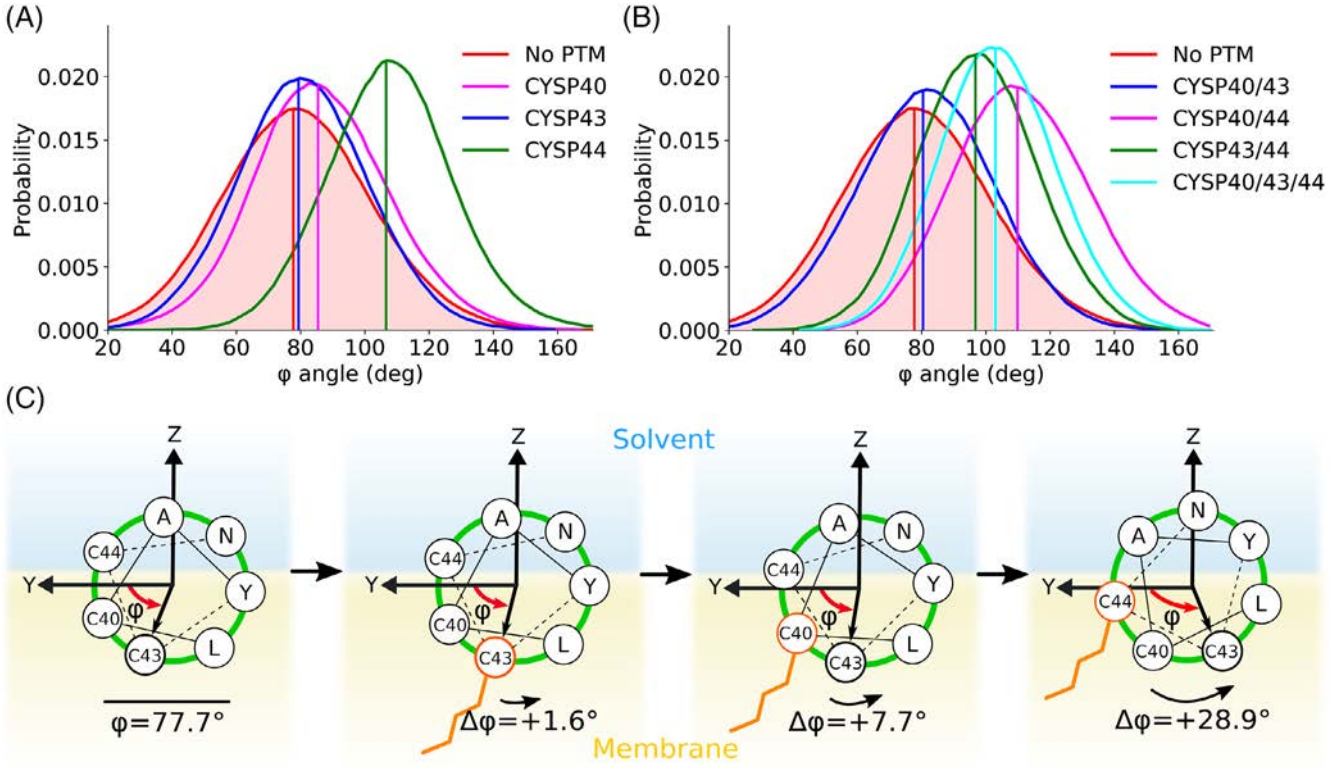

FIGURE 6 Effects of palmitoylation on orientation of the helix H2 relative to the membrane in coarse-grained simulations. Rotation of Cys43 relative to the membrane plane (**Y**) viewed from the N-terminus is analyzed. (A, B) Distributions for the Cys43 rotation angles relative to the membrane plane for different PTMs. Vertical lines indicate average values. (C) Schematics showing the H2 orientation with helical wheel projections for selected variants. Palmitoylation affects the orientation of H2 because the respective side chain becomes more hydrophobic

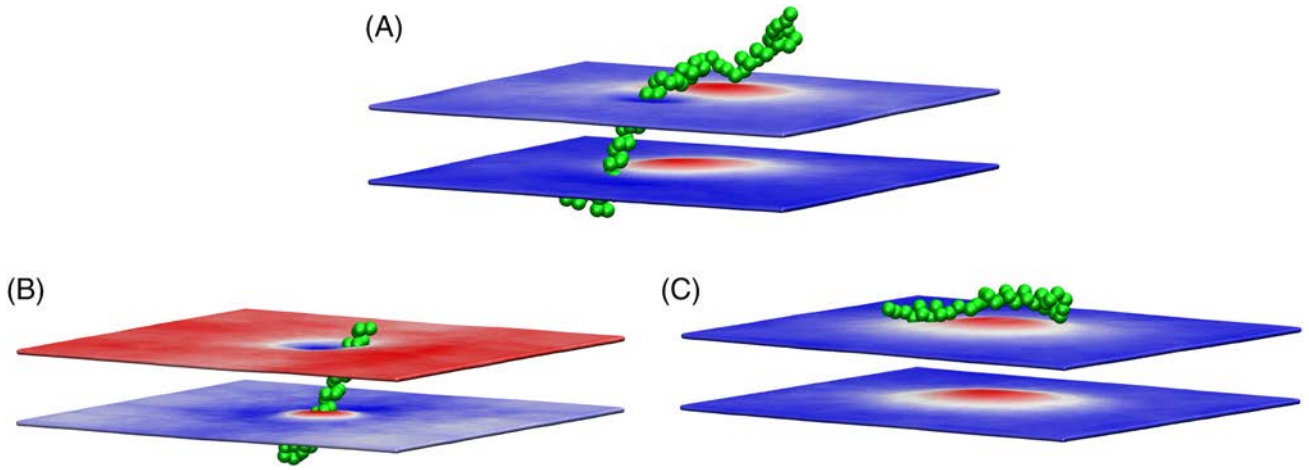

FIGURE 7 Induction of curvature by the E protein monomer in coarse grained (CG) simulations. Upward displacement of each membrane boundary is shown in red, and downward displacement is shown in blue. (A) Induction of curvature by the full-length E protein. (B) Membrane deformation by an isolated TMD. The membrane is thinned around the TMD, but no buckling is observed. (C) Membrane deformation by isolated H2 and H3 helices in CG simulation. The membrane is bent toward the α-helices H2 and H3. Each panel shows an exemplary protein position; positions of the membrane boundaries are averaged over the trajectory length

compared to the simulations of the monomeric protein (Figure S3). However, palmitoylation of Cys43 or Cys44 shifts the distribution of H2 positions ~2 Å closer to the membrane (Figure S9).

In all of the simulations of the pentameric E protein, we also observed bending of the membrane around it (Figure 9B). The mean curvature induced by the pentameric protein is roughly two times

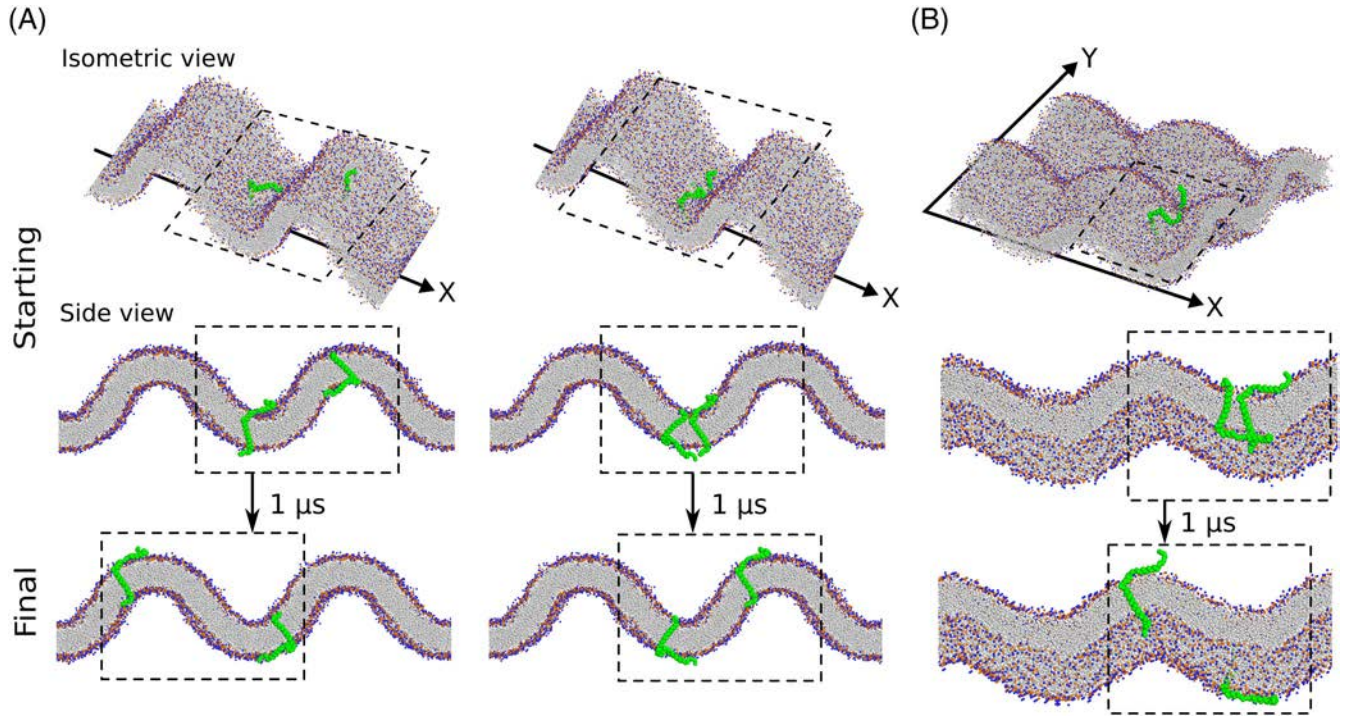

FIGURE 8 Monomeric E protein partitions into the curved region with the N-terminus localizing to the concave side independent of the starting position. (A) Simulations with the membrane buckled in one dimension. (B) Simulations with the membrane buckled in two dimensions. The dashed box shows the unit cell of the simulation

larger compared to the curvature induced by monomers (Figure S10). The obtained values of 0.05–0.1 nm^{-1} for the mean curvature imply the curvature radii of 10–20 nm.

3 | DISCUSSION

Coronaviruses have relatively large genomes harboring tens of different genes. Understanding of their structures could help in development of efficient antiviral measures. Yet some of the CoV proteins are transmembrane, and some contain intrinsically disordered regions,[64] at least until they become a part of a larger assembly. E protein has both properties: it has a TM segment, and it lacks tertiary structure in the monomeric form, while becoming more ordered in the pentameric assembly. Its flexibility and numerous CPTMs pose many problems for experimental studies, especially of the monomeric E protein. However, because it is small, and its properties are governed by basic physicochemical principles, it is a good subject for simulations.

Our results show that monomeric SARS-CoV-2 envelope protein has rich conformational dynamics strongly affected by CPTMs. The protein is organized as an α-helical TMD and two amphipathic α-helices H2 and H3, flanked by short disordered N- and C-termini. Whereas TMD is rigid and remains α-helical throughout the trajectories, helices H2 and H3 may partially unfold. TMD, H2, and H3 mostly move freely relative to each other, so the monomeric E protein can be considered a protein with intrinsically disordered regions. Yet, all of its α-helices have preferred orientations relative to the membrane.

The TM α-helix of the E protein is relatively long (28 amino acids, ~43 Å), and there is a mismatch between the length of its hydrophobic segment and the thickness of the hydrophobic region of the relevant membranes. Tilting of TM helices is a common mechanism for accommodating such mismatch.[65–69] Accordingly, we find that E protein TMD is tilted at 25–40°, similarly to TMD in pentameric E protein[57] and in other viroporins (Table S3). Besides tilting, the energetic costs of the hydrophobic mismatch can also be lowered by association (packing) of several TM helices.[70] In the case of the E protein, this mechanism could promote formation of pentamers. TMD also has a preferred azimuthal rotation angle, similarly to WALP peptides,[71,72] for which the results obtained with MD simulations were found to correspond well to those obtained in experiments.[73] However, the rotation angle of TMD in a free E protein monomer is opposite to that in the E protein pentamer. This is likely a consequence of the polar residues such as Glu8, Thr9, Thr11, Asn15, Ser16, Thr30, and Thr35 preferably facing the solvent in the monomer and interior of the channel in the pentamer.

One of the most potentially important findings is a strong dependence of the E protein structure on CPTMs. Previously, it was shown that palmitoylation is important for E protein stability and overall assembly of VLPs, whereas the role of glycosylation is more elusive.[17] Yet, experimental studies of the effects of CPTMs on protein structure are hindered by difficulties in obtaining homogeneous samples with a desired CPTM pattern; in vivo, palmitoylation is likely to be stochastic.[74] The proteins may be mutated to abolish the particular CPTM, however this may also introduce unintended side effects. On

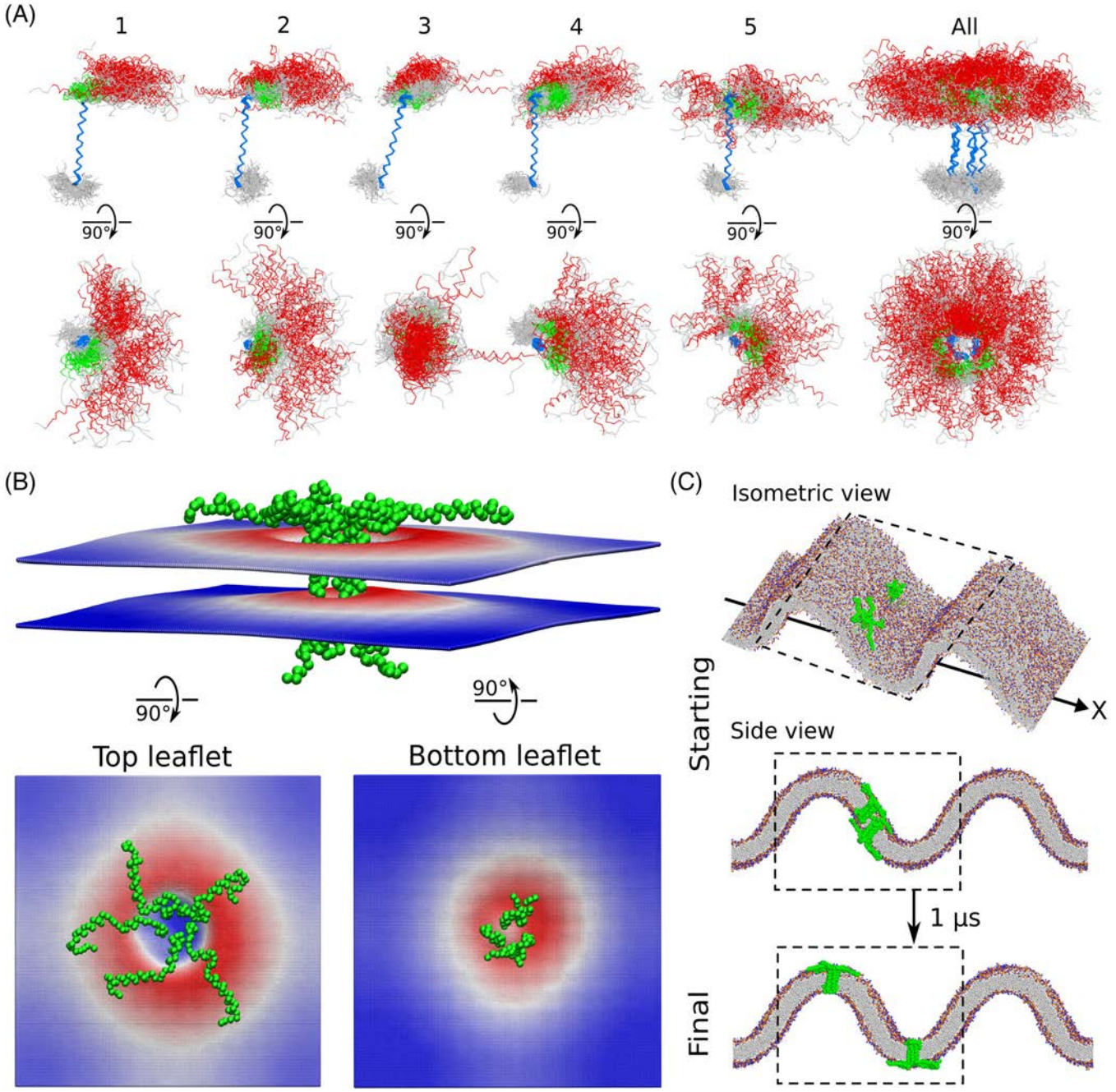

FIGURE 9 Properties of the pentameric E protein. (A) Conformations of the five protomers within the pentamer in 5 μs CG simulation based on the nuclear magnetic resonance model.[51] (B) Generation of curvature by pentameric E protein: the membrane bends toward the C-terminal helices H2 and H3. Upward displacement of each membrane boundary is shown in red, and downward displacement is shown in blue. Each panel shows an exemplary protein position; positions of the membrane boundaries are averaged over the trajectory length. (C) Repartitioning of the pentameric E protein into the curved region with the N-terminus localizing to the concave side independent of the starting position. The dashed box shows the unit cell of the simulation

the other hand, simulations allow for easier targeted testing of different defined combinations of CPTMs.

Previous structural studies of the E protein by NMR dealt with unmodified truncated variants. SARS-CoV E protein construct included residues 8–65, a His-tag and a linker; the cysteines were mutated to alanines, Asn66 was missing.[55,56] SARS-CoV-2 construct was even shorter (residues 8–38) and did not include the residues that could be modified.[50] Previous computational studies of the E protein also did not focus on the effects of CPTMs.[11,75,76] In this work, we found that the average orientation of H2 is strongly dependent on palmitoylation pattern, as the acyl chains act as anchors on the respective H2 cysteines and bring them closer to the membrane core. On the other hand, positioning of H3 is affected by glycosylation as the glycan acts as a buoy on H3 and

prevents its interaction with H2. However, most or all of the E proteins in vivo are probably not glycosylated,[27] so the possible role of this modification remains unclear. We believe that CPTMs are likely to elicit effects in the assembled oligomers similar to those that we observe in monomers.

In the last part of our work, we focused on interactions of the E protein with curved membranes. Overall, membrane curvature is an important factor in cell physiology,[77] being both generated and sensed by the major membrane constituents: lipids and proteins.[78,79] Some amphipathic α-helices are known to generate curvature by creating the area difference between the two leaflets of the bilayer[80,81] or to act as curvature sensors.[82,83]

Along with experiments, molecular dynamics simulations have also been fundamental in studies of curved membranes.[58] Earlier, simulations have been used to study repartitioning of both lipids and proteins in naturally and artificially curved membranes[60–63]; a prominent example is enrichment of cardiolipin and cholesterol in the regions with negative curvature.[60,62] Another example is the influenza A M2 protein, for which both experiments and simulations show that its amphiphilic α-helix induces membrane curvature, which is important for VLP budding and membrane scission,[84,85] and can act as a curvature sensor.[63]

Here, we have found that the SARS-CoV-2 E protein can generate membrane curvature, and this function can be ascribed to the amphiphilic C-terminal domain, containing α-helices H2 and H2 that insert into the proximal leaflet and cause its bulging. Such viroporin-generated curvature may stabilize the budding viral particle and promote its formation.[77] We have also found that the E protein can act as a curvature sensor and localize with the C-terminus at the convex regions of the membrane. Given that the C-terminus of E is oriented toward the cytoplasm,[27] the protein is likely to localize at the VLP budding sites and promote VLP budding. Concentration of the E protein in these curved areas may promote formation of pentameric channels. The assembled channels are also found to be curvature-sensitive due to their umbrella-like shape.[11,57] On the other hand, E protein is expected to be depleted at the concave inner surface of the VLP, in agreement with experimental data.[22,26,29–32]

Finally, we would like to discuss the limitations of the present study, and the future directions. First of all, we did not examine in detail the behavior of the envelope protein in the pentameric form. Root mean square deviations of the TM helix heavy atom positions between the available NMR models is above 6 Å.[51,57] Simulations performed by other laboratories reveal low stability of the pentameric models and frequent collapses of the pore.[76,86–88] Thus, behavior of the pentameric envelope protein deserves a very careful consideration. Perhaps, simulation of the pentamer assembly process starting from monomers or oligomers[89] would prove helpful in arriving at a satisfactory model. Furthermore, while we included the representative ERGIC lipids (POPC, POPE, POPI, POPS, and CHOL) in our simulations, and did not observe any specific interactions, there are many more lipid species in the cell membrane that might bind the envelope protein selectively, especially in the pentameric form, where it has larger accessible surface and, possibly, lipid-binding crevices. We also did not probe the interactions of the E protein with other coronaviral or cellular proteins; these interactions might have affected the structure and dynamics of the E protein. Future experimental and computational studies should provide a better picture of the E protein behavior in physiological settings.

4 | CONCLUSIONS

Our simulations show that the SARS-CoV-2 E protein in monomeric form has rich structural dynamics. The transmembrane helix is tilted in the membrane, and amphipathic helices move freely around it. Posttranslational palmitoylation anchors the helix H2 cysteines to the membrane. The E protein induces and senses membrane curvature, both in monomeric and pentameric forms.

These findings are in accordance with experimental observations, while providing a detailed description of the E protein structure. Our work showcases MD simulations as an important complementary technique allowing comprehensive inquiry in the case where the experiment is complicated: when the protein is partially disordered and may undergo different combinations of CPTMs.

We hope that our observations will help in understanding the role of the E protein in infection, in particular, by highlighting its membrane deformation abilities that should facilitate the budding of viral particles. The findings also explain the low abundance of the E protein in assembled virions. Finally, the data on the dynamics of the protein in monomeric form should be helpful for studying and elucidating its structure in physiological settings inside the infected cell, especially within the pentameric channels.

5 | METHODS

5.1 | Model preparation

As a starting structure for simulations of the monomeric and pentameric SARS-CoV-2 E protein, we used the model prepared by Heo and Feig[11] (https://github.com/feiglab/sars-cov-2-proteins/blob/master/Membrane/E_protein.pdb, accessed on September 1, 2020). Atomistic structure was converted into CG Martini 3 representation[90] using *martinize*. Define secondary structure of proteins (DSSP)[91,92] was used to assign the α-helical secondary structure for TMD, H2 and H3. The CG model was inserted into the POPC lipid bilayer using *insane*.[93] The structure of the monomer with CPTMs was constructed manually using PyMOL.[94] For further AA (all atom) simulations, CG structures were converted to AA using *backward*[95] and inserted into POPC or the native-like mixed bilayer composed of POPC/POPE/POPI/POPS/CHOL in the proportion 10:5:2:1:2 using CHARMM-GUI.[96]

In all simulations, the N- and C- termini, residues Lys, Arg, Asp, and Glu, and lipids POPS and POPI were charged. The membranes were solvated with water; counter ions were added to neutralize the systems. The simulations were performed using periodic boundary conditions. All systems were energy minimized using the steepest descent method,

equilibrated and simulated using GROMACS 2019.5 (AA) and GROMACS 2020.1 (CG).[97] To generate the buckled membranes, we compressed the bilayers in the *X*-dimension until reaching the desired strain by fixing the box size in these dimensions, while the membrane pressure coupling was turned off in the *X*-*Y* lateral dimensions.

5.2 | Simulation details

CG systems were simulated for 0.5, 1.0, or 2.0 μs (total simulation length > 10 μs), whereas each AA system was simulated 3 times for 100 ns (total simulation length 2.4 μs, Table S1). CG and AA simulations were conducted using the leapfrog integrator with time steps of 20 and 2 fs, at a reference temperature of 323 and 310 K, respectively, and at a reference pressure of 1 bar. Temperature was coupled using velocity rescale[98] and Nosé-Hoover[99] thermostats with coupling constant of 1 ps^{-1}, respectively. Pressure was coupled with semiisotropic Parrinello-Rahman barostat[100] with relaxation time of 12 or 5 ps, respectively.

5.3 | CG simulations

CG simulations were conducted using the beta version of Martini 3 force field with nonpolarizable water and optimized parameters for palmitoylated cysteines[101] and glycosylated asparagine[102] where needed. The center of mass of the reference structure was scaled with the scaling matrix of the pressure coupling. The nonbonded pair list was updated every 20 steps with the cutoff of 1.1 nm. Potentials shifted to zero at the cutoff of 1.1 nm and a reaction-field potential with $\varepsilon_{rf} = \infty$ were used for treatment of the van der Waals and electrostatics interactions.

5.4 | AA simulations

AA simulations were conducted using the CHARMM36m force field.[103] The covalent bonds to hydrogens were constrained using the LINear constraint solver (LINCS) algorithm.[104] The nonbonded pair list was updated every 20 steps with the cutoff of 1.2 nm. Force-based switching function with the switching range of 1.0–1.2 nm and particle mesh Ewald (PME) method with 0.12 nm Fourier grid spacing and 1.2 nm cutoff were used for treatment of the van der Waals and electrostatics interactions. The simulations were performed using JURECA.[105]

5.5 | Analysis

Visual molecular dynamics (VMD)[106] and in-house scripts were used for analysis of the TMD tilt angle (α) and rotational (azimuthal) angles (β, φ, ψ) of the TMD, H2, and H3. The tilt angle was defined as the angle between the TMD helix axis and the normal to the membrane (axis *Z*). The rotational angle was defined as the angle between the C_α radial vector of a reference residue (Phe23, Cys43, and Asn66) and the X–Z plane; the helix was aligned so that its axis was in the X–Z plane (Figures 5–7). We used the Ward's method from MDTraj[107] to group the dataset into four clusters based on pairwise root mean square deviation (RMSD) of coordinates of backbone particles. Density distributions of TMD, H2, and H3 atoms were calculated using the *density* tool from GROMACS. The secondary structure in the E protein was monitored using the *Timeline* plugin (version 2.3) for VMD.[106] PCA was performed on the positions of the C_α atoms (AA simulations) and backbone particles (CG simulations) using the *covar* and *anaeig* tools from GROMACS. Average positions of the membrane boundaries and curvature values were calculated using *g_lomepro*, version 1.0.2.[108]

ACKNOWLEDGMENTS

We are grateful to Pavel Buslaev for advices on using the Martini force field. The authors gratefully acknowledge the computing time granted through JARA on the supercomputer JURECA at Forschungszentrum Jülich. Ivan Gushchin was supported by the Ministry of Science and Higher Education of the Russian Federation (agreement #075-00337-20-03, project FSMG-2020-0003). Valentin Gordeliy and Roman Astashkin were supported by the Commissariat à l'Energie Atomique et aux Energies Alternatives (Institut de Biologie Structurale) – Helmholtz-Gemeinschaft Deutscher Forschungszentren (Forschungszentrum Jülich) Special Terms and Conditions 5.1 specific agreement.

CONFLICT OF INTEREST

The authors declare no competing interests.

AUTHOR CONTRIBUTIONS

Ivan Gushchin designed and supervised the project; Philipp Orekhov and Valentin Gordeliy helped with the project design; Alexander Kuzmin performed simulations with the help of Philipp Orekhov; Alexander Kuzmin and Ivan Gushchin analyzed the results and prepared the manuscript; Philipp Orekhov, Roman Astashkin, and Valentin Gordeliy helped with data analysis and manuscript preparation.

PEER REVIEW

The peer review history for this article is available at https://publons.com/publon/10.1002/prot.26317.

DATA AVAILABILITY STATEMENT

Molecular dynamics trajectories have been deposited to Zenodo and are available using the following links: https://doi.org/10.5281/zenodo.4740706 (CG simulations of monomeric protein); https://doi.org/10.5281/zenodo.4743386 (AA simulations of monomeric protein); https://doi.org/10.5281/zenodo.5232499 (CG simulations of pentameric protein).

ORCID

Alexander Kuzmin https://orcid.org/0000-0003-3945-3691
Philipp Orekhov https://orcid.org/0000-0003-4078-4762
Roman Astashkin https://orcid.org/0000-0001-9065-8225
Valentin Gordeliy https://orcid.org/0000-0001-5782-5896
Ivan Gushchin https://orcid.org/0000-0002-5348-6070

REFERENCES

1. Fehr AR, Perlman S. Coronaviruses: an overview of their replication and pathogenesis. In: Maier HJ, Bickerton E, Britton P, eds. *Coronaviruses: Methods and Protocols*. Springer; 2015:1-23. doi: 10.1007/978-1-4939-2438-7_1
2. Gorbalenya AE, Baker SC, Baric RS, et al. Coronaviridae Study Group of the International Committee on taxonomy of viruses, the species severe acute respiratory syndrome-related coronavirus: classifying 2019-nCoV and naming it SARS-CoV-2. *Nat Microbiol*. 2020;5:536-544. doi:10.1038/s41564-020-0695-z
3. Cui J, Li F, Shi Z-L. Origin and evolution of pathogenic coronaviruses. *Nat Rev Microbiol*. 2019;17:181-192. doi:10.1038/s41579-018-0118-9
4. Hu B, Guo H, Zhou P, Shi Z-L. Characteristics of SARS-CoV-2 and COVID-19. *Nat Rev Microbiol*. 2020;19:1-14. doi:10.1038/s41579-020-00459-7
5. Bárcena M, Barnes CO, Beck M, et al. Structural biology in the fight against COVID-19. *Nat Struct Mol Biol*. 2021;28:2-7. doi: 10.1038/s41594-020-00544-8
6. Arantes PR, Saha A, Palermo G. Fighting COVID-19 using molecular dynamics simulations. *ACS Cent Sci*. 2020;6:1654-1656. doi: 10.1021/acscentsci.0c01236
7. Mulholland AJ, Amaro RE. COVID19—computational chemists meet the moment. *J Chem Inf Model*. 2020;60:5724-5726. doi: 10.1021/acs.jcim.0c01395
8. Zimmerman MI, Porter JR, Ward MD, et al. SARS-CoV-2 simulations go Exascale to capture spike opening and reveal cryptic pockets across the proteome. *Nat Chem*. 2021;13(7):651-659. doi: 10.1101/2020.06.27.175430
9. Casalino L, Gaieb Z, Goldsmith JA, et al. Beyond shielding: the roles of glycans in the SARS-CoV-2 spike protein. *ACS Cent Sci*. 2020;6: 1722-1734. doi:10.1021/acscentsci.0c01056
10. Yu A, Pak AJ, He P, et al. A multiscale coarse-grained model of the SARS-CoV-2 virion. *Biophys J*. 2020;120(6):1097-1104. doi: 10.1016/j.bpj.2020.10.048
11. Heo L, Feig M. Modeling of severe acute respiratory syndrome coronavirus 2 (SARS-CoV-2) proteins by machine learning and physics-based refinement. *BioRxiv*. 2020;2020.03.25.008904. doi: 10.1101/2020.03.25.008904
12. Chodera J, Lee AA, London N, von Delft F. Crowdsourcing drug discovery for pandemics. *Nat Chem*. 2020;12:581-581. doi: 10.1038/s41557-020-0496-2
13. T.C.M. Consortium, Achdout H, Aimon A, et al. COVID moonshot: Open Science discovery of SARS-CoV-2 Main protease inhibitors by combining crowdsourcing, high-throughput experiments, computational simulations, and machine learning. *BioRxiv*. 2020; 2020.10.29.339317. doi:10.1101/2020.10.29.339317
14. Masters PS. The molecular biology of coronaviruses. *Advances in Virus Research*. Cambridge, MA: Academic Press; 2006:193-292. doi: 10.1016/S0065-3527(06)66005-3
15. Nieto-Torres JL, DeDiego ML, Verdiá-Báguena C, et al. Severe acute respiratory syndrome coronavirus envelope protein ion channel activity promotes virus fitness and pathogenesis. *PLoS Pathog*. 2014; 10:e1004077. doi:10.1371/journal.ppat.1004077
16. Ruch TR, Machamer CE. The coronavirus E protein: assembly and beyond. *Viruses*. 2012;4:363-382. doi:10.3390/v4030363
17. Schoeman D, Fielding BC. Coronavirus envelope protein: current knowledge. *Virol J*. 2019;16:69. doi:10.1186/s12985-019-1182-0
18. Petit CM, Chouljenko VN, Iyer A, et al. Palmitoylation of the cysteine-rich endodomain of the SARS–coronavirus spike glycoprotein is important for spike-mediated cell fusion. *Virology*. 2007;360: 264-274. doi:10.1016/j.virol.2006.10.034
19. Fujiwara Y, Kondo HX, Shirota M, et al. Structural basis for the membrane association of ankyrinG via palmitoylation. *Sci Rep*. 2016;6: 23981. doi:10.1038/srep23981
20. Sobocińska J, Roszczenko-Jasińska P, Ciesielska A, Kwiatkowska K. Protein palmitoylation and its role in bacterial and viral infections. *Front Immunol*. 2018;8:2003. doi: 10.3389/fimmu.2017.02003
21. Boscarino JA, Logan HL, Lacny JJ, Gallagher TM. Envelope protein palmitoylations are crucial for murine coronavirus assembly. *J Virol*. 2008;82:2989-2999. doi:10.1128/JVI.01906-07
22. Lopez LA, Riffle AJ, Pike SL, Gardner D, Hogue BG. Importance of conserved cysteine residues in the coronavirus envelope protein. *J Virol*. 2008;82:3000-3010. doi:10.1128/JVI.01914-07
23. Yuan Q, Liao Y, Torres J, Tam JP, Liu DX. Biochemical and functional characterization of the membrane association and membrane permeabilizing activity of the severe acute respiratory syndrome coronavirus envelope protein. *Virology*. 2006;349:264-275. doi: 10.1016/j.virol.2006.01.028
24. Grant OC, Montgomery D, Ito K, Woods RJ. Analysis of the SARS-CoV-2 spike protein glycan shield reveals implications for immune recognition. *Sci Rep*. 2020;10:14991. doi:10.1038/s41598-020-71748-7
25. Marth JD, Grewal PK. Mammalian glycosylation in immunity. *Nat Rev Immunol*. 2008;8:874-887. doi:10.1038/nri2417
26. Nieto-Torres JL, DeDiego ML, Álvarez E, et al. Subcellular location and topology of severe acute respiratory syndrome coronavirus envelope protein. *Virology*. 2011;415:69-82. doi:10.1016/j.virol.2011.03.029
27. Duart G, García-Murria MJ, Grau B, Acosta-Cáceres JM, Martínez-Gil L, Mingarro I. SARS-CoV-2 envelope protein topology in eukaryotic membranes. *Open Biol*. 2020;10:200209. doi: 10.1098/rsob.200209
28. Duart G, García-Murria MJ, Mingarro I. The SARS-CoV-2 envelope (E) protein has evolved towards membrane topology robustness. *Biochim Biophys Acta Biomembr*. 2021;1863:183608. doi:10.1016/j.bbamem.2021.183608
29. Boson B, Legros V, Zhou B, et al. The SARS-CoV-2 envelope and membrane proteins modulate maturation and retention of the spike protein, allowing assembly of virus-like particles. *J Biol Chem*. 2021; 296:100111. doi:10.1074/jbc.RA120.016175
30. Cohen JR, Lin LD, Machamer CE. Identification of a Golgi complex-targeting signal in the cytoplasmic tail of the severe acute respiratory syndrome coronavirus envelope protein. *J Virol*. 2011;85:5794-5803. doi:10.1128/JVI.00060-11
31. Godet M, L'Haridon R, Vautherot J-F, Laude H. TGEV corona virus ORF4 encodes a membrane protein that is incorporated into virions. *Virology*. 1992;188:666-675. doi:10.1016/0042-6822(92)90521-P
32. Venkatagopalan P, Daskalova SM, Lopez LA, Dolezal KA, Hogue BG. Coronavirus envelope (E) protein remains at the site of assembly. *Virology*. 2015;478:75-85. doi:10.1016/j.virol.2015.02.005
33. Appenzeller-Herzog C, Hauri H-P. The ER-golgi intermediate compartment (ERGIC): in search of its identity and function. *J Cell Sci*. 2006;119:2173-2183. doi:10.1242/jcs.03019
34. Ortego J, Ceriani JE, Patiño C, Plana J, Enjuanes L. Absence of E protein arrests transmissible gastroenteritis coronavirus maturation in the secretory pathway. *Virology*. 2007;368:296-308. doi:10.1016/j.virol.2007.05.032
35. Fischer F, Stegen CF, Masters PS, Samsonoff WA. Analysis of constructed E gene mutants of mouse hepatitis virus confirms a pivotal role for E protein in coronavirus assembly. *J Virol*. 1998;72:7885-7894. doi:10.1128/JVI.72.10.7885-7894.1998
36. Corse E, Machamer CE. The cytoplasmic tails of infectious bronchitis virus E and M proteins mediate their interaction. *Virology*. 2003;312: 25-34. doi:10.1016/S0042-6822(03)00175-2
37. Tseng Y-T, Wang S-M, Huang K-J, Wang C-T. SARS-CoV envelope protein palmitoylation or nucleocapid association is not required for promoting virus-like particle production. *J Biomed Sci*. 2014;21:34. doi:10.1186/1423-0127-21-34

38. Álvarez E, DeDiego ML, Nieto-Torres JL, Jiménez-Guardeño JM, Marcos-Villar L, Enjuanes L. The envelope protein of severe acute respiratory syndrome coronavirus interacts with the non-structural protein 3 and is ubiquitinated. *Virology*. 2010;402:281-291. doi: 10.1016/j.virol.2010.03.015
39. Xu R, Shi M, Li J, Song P, Li N. Construction of SARS-CoV-2 virus-like particles by mammalian expression system. *Front Bioeng Biotechnol*. 2020;8. doi:10.3389/fbioe.2020.00862
40. Yang Y, Xiong Z, Zhang S, et al. Bcl-xL inhibits T-cell apoptosis induced by expression of SARS coronavirus E protein in the absence of growth factors. *Biochem J*. 2005;392:135-143. doi: 10.1042/BJ20050698
41. Teoh K-T, Siu Y-L, Chan W-L, et al. The SARS coronavirus E protein interacts with PALS1 and alters tight junction formation and epithelial morphogenesis. *Mol Biol Cell*. 2010;21:3838-3852. doi: 10.1091/mbc.E10-04-0338
42. Toto A, Ma S, Malagrinò F, et al. Comparing the binding properties of peptides mimicking the envelope protein of SARS-CoV and SARS-CoV-2 to the PDZ domain of the tight junction-associated PALS1 protein. *Protein Sci*. 2020;29:2038-2042. doi: 10.1002/pro.3936
43. Gordon DE, Jang GM, Bouhaddou M, et al. A SARS-CoV-2 protein interaction map reveals targets for drug repurposing. *Nature*. 2020; 583:459-468. doi:10.1038/s41586-020-2286-9
44. Verdiá-Báguena C, Nieto-Torres JL, Alcaraz A, et al. Coronavirus E protein forms ion channels with functionally and structurally-involved membrane lipids. *Virology*. 2012;432:485-494. doi: 10.1016/j.virol.2012.07.005
45. Parthasarathy K, Ng L, Lin X, et al. Structural flexibility of the pentameric SARS coronavirus envelope protein ion channel. *Biophys J*. 2008;95:L39-L41. doi:10.1529/biophysj.108.133041
46. Surya W, Li Y, Verdià-Bàguena C, Aguilella VM, Torres J. MERS coronavirus envelope protein has a single transmembrane domain that forms pentameric ion channels. *Virus Res*. 2015;201:61-66. doi: 10.1016/j.virusres.2015.02.023
47. Singh Tomar PP, Arkin IT. SARS-CoV-2 E protein is a potential ion channel that can be inhibited by gliclazide and memantine. *Biochem Biophys Res Commun*. 2020;530:10-14. doi:10.1016/j.bbrc.2020.05.206
48. Wilson L, Gage P, Ewart G. Hexamethylene amiloride blocks E protein ion channels and inhibits coronavirus replication. *Virology*. 2006; 353:294-306. doi:10.1016/j.virol.2006.05.028
49. Pervushin K, Tan E, Parthasarathy K, et al. Structure and inhibition of the SARS coronavirus envelope protein ion channel. *PLoS Pathog*. 2009;5:e1000511. doi:10.1371/journal.ppat.1000511
50. Torres J, Maheswari U, Parthasarathy K, Ng L, Liu DX, Gong X. Conductance and amantadine binding of a pore formed by a lysine-flanked transmembrane domain of SARS coronavirus envelope protein. *Protein Sci*. 2007;16:2065-2071. doi:10.1110/ps.062730007
51. Mandala VS, McKay MJ, Shcherbakov AA, Dregni AJ, Kolocouris A, Hong M. Structure and drug binding of the SARS-CoV-2 envelope protein transmembrane domain in lipid bilayers. *Nat Struct Mol Biol*. 2020;27:1202-1208. doi:10.1038/s41594-020-00536-8
52. To J, Surya W, Torres J. Chapter eight—targeting the channel activity of Viroporins. In: Donev R, ed. *Advances in Protein Chemistry and Structural Biology*. Vol 104. Academic Press; 2016:307-355. doi: 10.1016/bs.apcsb.2015.12.003
53. Nieva JL, Madan V, Carrasco L. Viroporins: structure and biological functions. *Nat Rev Microbiol*. 2012;10:563-574. doi: 10.1038/nrmicro2820
54. Jefferson T, Deeks J, Demicheli V, Rivetti D, Rudin M. Amantadine and rimantadine for preventing and treating influenza a in adults. *Cochrane Database Syst Rev*. 2004;2:CD001169. doi: 10.1002/14651858.CD001169.pub2
55. Nieto-Torres JL, Verdiá-Báguena C, Jimenez-Guardeño JM, et al. Severe acute respiratory syndrome coronavirus E protein transports calcium ions and activates the NLRP3 inflammasome. *Virology*. 2015;485:330-339. doi:10.1016/j.virol.2015.08.010
56. Li Y, Surya W, Claudine S, Torres J. Structure of a conserved Golgi complex-targeting signal in coronavirus envelope proteins. *J Biol Chem*. 2014;289:12535-12549. doi:10.1074/jbc.M114.560094
57. Surya W, Li Y, Torres J. Structural model of the SARS coronavirus E channel in LMPG micelles. *Biochim Biophys Acta Biomembr*. 2018; 1860:1309-1317. doi:10.1016/j.bbamem.2018.02.017
58. Marrink SJ, de Vries AH, Tieleman DP. Lipids on the move: simulations of membrane pores, domains, stalks and curves. *Biochim Biophys Acta*. 2009;1788:149-168. doi:10.1016/j.bbamem.2008.10.006
59. Buslaev P, Gushchin I. Effects of coarse graining and saturation of hydrocarbon chains on structure and dynamics of simulated lipid molecules. *Sci Rep*. 2017;7:11476. doi:10.1038/s41598-017-11761-5
60. Boyd KJ, Alder NN, May ER. Buckling under pressure: curvature-based lipid segregation and stability modulation in Cardiolipin-containing bilayers. *Langmuir*. 2017;33:6937-6946. doi:10.1021/acs.langmuir.7b01185
61. Elías-Wolff F, Lindén M, Lyubartsev AP, Brandt EG. Computing curvature sensitivity of biomolecules in membranes by simulated buckling. *J Chem Theory Comput*. 2018;14:1643-1655. doi:10.1021/acs.jctc.7b00878
62. Baoukina S, Ingólfsson HI, Marrink SJ, Tieleman DP. Curvature-induced sorting of lipids in plasma membrane tethers. *Adv Theory Simul*. 2018;1:1800034. doi:10.1002/adts.201800034
63. Madsen JJ, Grime JMA, Rossman JS, Voth GA. Entropic forces drive clustering and spatial localization of influenza a M2 during viral budding. *Proc Natl Acad Sci USA*. 2018;115:E8595-E8603. doi: 10.1073/pnas.1805443115
64. Giri R, Bhardwaj T, Shegane M, et al. Understanding COVID-19 via comparative analysis of dark proteomes of SARS-CoV-2, human SARS and bat SARS-like coronaviruses. *Cell Mol Life Sci*. 2020;78: 1655-1688. doi:10.1007/s00018-020-03603-x
65. Park SH, Opella SJ. Tilt angle of a trans-membrane helix is determined by hydrophobic mismatch. *J Mol Biol*. 2005;350:310-318. doi: 10.1016/j.jmb.2005.05.004
66. Kandasamy SK, Larson RG. Molecular dynamics simulations of model trans-membrane peptides in lipid bilayers: a systematic investigation of hydrophobic mismatch. *Biophys J*. 2006;90:2326-2343. doi: 10.1529/biophysj.105.073395
67. Özdirekcan S, Etchebest C, Killian JA, Fuchs PFJ. On the orientation of a designed transmembrane peptide: toward the right tilt angle? *J Am Chem Soc*. 2007;129:15174-15181. doi:10.1021/ja073784q
68. Duong-Ly KC, Nanda V, DeGrado WF, Howard KP. The conformation of the pore region of the M2 proton channel depends on lipid bilayer environment. *Protein Sci*. 2005;14:856-861. doi: 10.1110/ps.041185805
69. Koehorst RBM, Spruijt RB, Vergeldt FJ, Hemminga MA. Lipid bilayer topology of the transmembrane α-helix of M13 major coat protein and bilayer polarity profile by site-directed fluorescence spectroscopy. *Biophys J*. 2004;87:1445-1455. doi: 10.1529/biophysj.104.043208
70. Benjamini A, Smit B. Robust driving forces for transmembrane helix packing. *Biophys J*. 2012;103:1227-1235. doi:10.1016/j.bpj.2012.08.035
71. Holt A, Killian JA. Orientation and dynamics of transmembrane peptides: the power of simple models. *Eur Biophys J*. 2010;39:609-621. doi:10.1007/s00249-009-0567-1
72. Kim T, Im W. Revisiting hydrophobic mismatch with free energy simulation studies of transmembrane helix tilt and rotation. *Biophys J*. 2010;99:175-183. doi:10.1016/j.bpj.2010.04.015
73. Strandberg E, Esteban-Martín S, Ulrich AS, Salgado J. Hydrophobic mismatch of mobile transmembrane helices: merging theory and

experiments. *Biochim Biophys Acta Biomembr*. 2012;1818:1242-1249. doi:10.1016/j.bbamem.2012.01.023
74. Rodenburg RNP, Snijder J, van de Waterbeemd M, et al. Stochastic palmitoylation of accessible cysteines in membrane proteins revealed by native mass spectrometry. *Nat Commun*. 2017;8:1280. doi:10.1038/s41467-017-01461-z
75. Sarkar M, Saha S. Structural insight into the role of novel SARS-CoV-2 E protein: a potential target for vaccine development and other therapeutic strategies. *PLoS One*. 2020;15:e0237300. doi:10.1371/journal.pone.0237300
76. Cao Y, Yang R, Wang W, et al. Computational study of the ion and water permeation and transport mechanisms of the SARS-CoV-2 pentameric E protein channel. *Front Mol Biosci*. 2020;7. doi:10.3389/fmolb.2020.565797
77. McMahon HT, Boucrot E. Membrane curvature at a glance. *J Cell Sci*. 2015;128:1065-1070. doi:10.1242/jcs.114454
78. Graham TR, Kozlov MM. Interplay of proteins and lipids in generating membrane curvature. *Curr Opin Cell Biol*. 2010;22:430-436. doi:10.1016/j.ceb.2010.05.002
79. Baumgart T, Capraro BR, Zhu C, Das SL. Thermodynamics and mechanics of membrane curvature generation and sensing by proteins and lipids. *Annu Rev Phys Chem*. 2011;62:483-506. doi:10.1146/annurev.physchem.012809.103450
80. Jarsch IK, Daste F, Gallop JL. Membrane curvature in cell biology: an integration of molecular mechanisms. *J Cell Biol*. 2016;214:375-387. doi:10.1083/jcb.201604003
81. Campelo F, McMahon HT, Kozlov MM. The hydrophobic insertion mechanism of membrane curvature generation by proteins. *Biophys J*. 2008;95:2325-2339. doi:10.1529/biophysj.108.133173
82. Drin G, Casella J-F, Gautier R, Boehmer T, Schwartz TU, Antonny B. A general amphipathic α-helical motif for sensing membrane curvature. *Nat Struct Mol Biol*. 2007;14:138-146. doi:10.1038/nsmb1194
83. Cui H, Lyman E, Voth GA. Mechanism of membrane curvature sensing by amphipathic helix containing proteins. *Biophys J*. 2011;100:1271-1279. doi:10.1016/j.bpj.2011.01.036
84. Schmidt NW, Wong GCL. Antimicrobial peptides and induced membrane curvature: geometry, coordination chemistry, and molecular engineering. *Curr Opin Solid State Mater Sci*. 2013;17:151-163. doi:10.1016/j.cossms.2013.09.004
85. Rossman JS, Jing X, Leser GP, Lamb RA. Influenza virus M2 protein mediates ESCRT-independent membrane scission. *Cell*. 2010;142:902-913. doi:10.1016/j.cell.2010.08.029
86. Mehregan A, Pérez-Conesa S, Zhuang Y, et al. Biophysical characterization of the SARS-CoV-2 E protein. *bioRXiv*. 2021. doi:10.1101/2021.05.28.446179
87. Monje-Galvan V, Voth GA. Molecular interactions of the M and E integral membrane proteins of SARS-CoV-2. *Faraday Discuss*. 2021;232:49-67. doi:10.1039/D1FD00031D
88. Sun S, Karki C, Aguilera J, Lopez Hernandez AE, Sun J, Li L. Computational study on the function of palmitoylation on the envelope protein in SARS-CoV-2. *J Chem Theory Comput*. 2021;17:6483-6490. doi:10.1021/acs.jctc.1c00359
89. Novitskaia O, Buslaev P, Gushchin I. Assembly of spinach chloroplast ATP synthase rotor ring protein-lipid complex. *Front Mol Biosci*. 2019;6. doi:10.3389/fmolb.2019.00135
90. Souza PCT, Thallmair S, Conflitti P, et al. Protein–ligand binding with the coarse-grained martini model. *Nat Commun*. 2020;11:3714. doi:10.1038/s41467-020-17437-5
91. Touw WG, Baakman C, Black J, et al. A series of PDB-related databanks for everyday needs. *Nucleic Acids Res*. 2015;43:D364-D368. doi:10.1093/nar/gku1028
92. Kabsch W, Sander C. Dictionary of protein secondary structure: pattern recognition of hydrogen-bonded and geometrical features. *Biopolymers*. 1983;22:2577-2637. doi:10.1002/bip.360221211
93. Wassenaar TA, Ingólfsson HI, Böckmann RA, Tieleman DP, Marrink SJ. Computational lipidomics with insane: a versatile tool for generating custom membranes for molecular simulations. *J Chem Theory Comput*. 2015;11:2144-2155. doi:10.1021/acs.jctc.5b00209
94. DeLano WL. *The PyMOL Molecular Graphics System*. Delano Scientific; 2002.
95. Wassenaar TA, Pluhackova K, Böckmann RA, Marrink SJ, Tieleman DP. Going backward: a flexible geometric approach to reverse transformation from coarse grained to atomistic models. *J Chem Theory Comput*. 2014;10:676-690. doi:10.1021/ct400617g
96. Jo S, Kim T, Iyer VG, Im W. CHARMM-GUI: a web-based graphical user interface for CHARMM. *J Comput Chem*. 2008;29:1859-1865. doi:10.1002/jcc.20945
97. Abraham MJ, Murtola T, Schulz R, et al. GROMACS: high performance molecular simulations through multi-level parallelism from laptops to supercomputers. *SoftwareX*. 2015;1–2:19-25. doi:10.1016/j.softx.2015.06.001
98. Bussi G, Donadio D, Parrinello M. Canonical sampling through velocity rescaling. *J Chem Phys*. 2007;126:014101. doi:10.1063/1.2408420
99. Nosé S. A unified formulation of the constant temperature molecular dynamics methods. *J Chem Phys*. 1984;81:511-519. doi:10.1063/1.447334
100. Parrinello M, Rahman A. Polymorphic transitions in single crystals: a new molecular dynamics method. *J Appl Phys*. 1981;52:7182-7190. doi:10.1063/1.328693
101. Atsmon-Raz Y, Tieleman DP. Parameterization of palmitoylated cysteine, farnesylated cysteine, geranylgeranylated cysteine, and myristoylated glycine for the martini force field. *J Phys Chem B*. 2017;121:11132-11143. doi:10.1021/acs.jpcb.7b10175
102. Shivgan AT, Marzinek JK, Huber RG, et al. Extending the martini coarse-grained force field to N-glycans. *J Chem Inf Model*. 2020;60:3864-3883. doi:10.1021/acs.jcim.0c00495
103. Huang J, Rauscher S, Nawrocki G, et al. CHARMM36m: an improved force field for folded and intrinsically disordered proteins. *Nat Methods*. 2017;14:71-73. doi:10.1038/nmeth.4067
104. Hess B, Bekker H, Berendsen H, Fraaije J. LINCS: a linear constraint solver for molecular simulations. *J Comput Chem*. 1997;18:1463-1472. doi:10.1002/(sici)1096-987x(199709)18:12%3C1463::aid-jcc4%3E3.0.co;2-h
105. Krause D, Thörnig P. JURECA: modular supercomputer at Jülich supercomputing centre. *J Large-Scale Res Facilit*. 2018;4:132. doi:10.17815/jlsrf-4-121-1
106. Humphrey W, Dalke A, Schulten K. VMD visual molecular dynamics. *J Mol Graph*. 1996;14:33-38. doi:10.1016/0263-7855(96)00018-5
107. McGibbon RT, Beauchamp KA, Harrigan MP, et al. MDTraj: a modern open library for the analysis of molecular dynamics trajectories. *Biophys J*. 2015;109:1528-1532. doi:10.1016/j.bpj.2015.08.015
108. Gapsys V, de Groot BL, Briones R. Computational analysis of local membrane properties. *J Comput Aided Mol Des*. 2013;27:845-858. doi:10.1007/s10822-013-9684-0

Structure and dynamics of the SARS-CoV-2 envelope protein monomer

Alexander Kuzmin, Philipp Orekhov, Roman Astashkin, Valentin Gordeliy, Ivan Gushchin*

E-mail for correspondence: ivan.gushchin@phystech.edu

Supporting Information

Supporting Text

Supporting Tables S1-S3

Supporting Figures S1-S10

Supporting References

Supporting Text

Effect of glycosylation on helix H3

As shown previously [1,2], E protein may be glycosylated. There are two potential glycosylation sites: Asn48 and Asn66, yet the former is too close to the membrane to be efficiently glycosylated [2], and its mutation to aspartate didn't change the glycosylation pattern [1]. Here, we find that glycosylation of Asn66 has a pronounced effect on dynamics of the helix H3 (Figure S4). In the unmodified protein, we observed two major orientations of H3: the first one with the hydrophobic residues Val62 and Leu65 facing the membrane, and the less frequent orientation almost completely opposite to it, with H3 stacking with H2 while being slightly above it (Figure S4). Glycosylation resulted in abolishment of the second orientation, presumably due to the potential steric conflict between the sugar moiety and H2 (Figure S4A,D); the helix was also slightly rotated in the most frequent orientation (Figure S4A,E).

Table S1. List of the simulated systems and their properties.

№	Type	Protein	Number of lipids (by leaflet)	Number of waters	Number of ions (0.15 mM)	Time, μs	Simulation box size, nm^3
1, 2	CG	No PTM	POPC (206/221)	7706	Na+(84) Cl-(86)	2, 0.5	12×12×11 (rectangular)
3	CG	CYSP40	POPC (205/221)	7711	Na+(84) Cl-(86)	0.5	12×12×11 (rectangular)
4	CG	CYSP43	POPC (206/221)	7580	Na+(82) Cl-(84)	0.5	12×12×11 (rectangular)
5	CG	CYSP44	POPC (205/221)	7609	Na+(83) Cl-(85)	0.5	12×12×11 (rectangular)
6	CG	CYSP40/43	POPC (206/221)	7599	Na+(83) Cl-(85)	0.5	12×12×11 (rectangular)
7	CG	CYSP40/44	POPC (205/220)	7605	Na+(83) Cl-(85)	0.5	12×12×11 (rectangular)
8	CG	CYSP43/44	POPC (204/221)	7600	Na+(83) Cl-(85)	0.5	12×12×11 (rectangular)
9	CG	CYSP40/43/44	POPC (205/219)	7616	Na+(83) Cl-(85)	0.5	12×12×11 (rectangular)
10	CG	ASNG66	POPC (202/221)	12709	Na+(139) Cl-(141)	0.5	12×12×15 (rectangular)
11	CG	TMD, no PTM	POPC (222/219)	7934	Na+(88) Cl-(86)	0.5	12×12×11 (rectangular)
12	CG	H2+H3, no PTM	POPC (207/225)	7654	Na+(82) Cl-(86)	0.5	12×12×11 (rectangular)
13	AA	No PTM (1)	POPC (174/180)	31286	Na+(84) Cl-(86)	0.1×3	11×11×12 (hexagonal)
14	AA	No PTM (2)	POPC (171/179)	31304	Na+(85) Cl-(87)	0.1×3	11×11×12 (hexagonal)
15	AA	No PTM (3)	POPC (169/179)	30882	Na+(84) Cl-(86)	0.1×3	11×11×12 (hexagonal)
16	AA	No PTM (4)	POPC (174/179)	31104	Na+(84) Cl-(86)	0.1×3	11×11×12 (hexagonal)

17	AA	No PTM (1)	Mixture: POPC (100/100), POPE (50/50), POPI (20/20), POPS (10/10), CHOL (20/20)	34215	Na+(151) Cl-(93)	0.1×3	11×11×12 (hexagonal)
18	AA	No PTM (2)		32677	Na+(146) Cl-(88)	0.1×3	11×11×12 (hexagonal)
19	AA	No PTM (3)		32243	Na+(145) Cl-(87)	0.1×3	11×11×12 (hexagonal)
20	AA	No PTM (4)		35190	Na+(155) Cl-(97)	0.1×3	11×11×12 (hexagonal)
21, 22	CG	1D buckled along X axis 2×No PTM	POPC (946/950)	64695	Na+(710) Cl-(714)	1	25×20×21 (rectangular)
23	CG	2D buckled along X, Y 2×No PTM	POPC (759/761)	52249	Na+(573) Cl-(577)	1	21×21×20 (rectangular)
24	CG	4×No PTM	POPC (3998/3997)	105411	Na+(10493) Cl-(10501)	1	50×50×10 (rectangular)
25	CG	Pentamer No PTM (Feig lab)	POPC (374/425)	17252	Na+(185) Cl-(195)	5	17×17×12 (rectangular)
26	CG	Pentamer No PTM (Feig lab + NMR TMD)	POPC (373/431)	17274	Na+(185) Cl-(195)	5	17×17×12 (rectangular)
27	CG	Pentamer CYSP43	POPC (376/423)	17196	Na+(184) Cl-(194)	5	17×17×12 (rectangular)
28	CG	Pentamer CYSP44	POPC (375/421)	17240	Na+(185) Cl-(195)	5	17×17×12 (rectangular)
29	CG	1D buckled along X-axis 2×Pentamer No PTM (Feig lab)	POPC (2184/2185)	135702	Na+(1484) Cl-(1504)	1	36×30×21 (rectangular)

Table S2. Average values and standard deviations (σ) of the tilt and rotation angles of TMD and H2 observed in different simulations. See Figures 5 and 6 for definitions.

Type	**System**	**Lipid**	**Mean α, °**	**σ_α, °**	**Mean β, °**	**σ_β, °**	**Mean φ, °**	**Δφ, °**	**σ_φ, °**
CG	No PTM	POPC	26.9	8	34.1	29.4	77.7		22.5
CG	CYSP40	POPC	26.6	8.9	34.7	31.2	85.4	+7.7	20.5
CG	CYSP43	POPC	26.7	8.4	32.4	29	79.3	+1.6	19.7
CG	CYSP44	POPC	27.1	8.3	40.3	28.8	106.6	+28.9	19.1
CG	CYSP40/43	POPC	27.7	8.9	34.8	30.9	80.4	+2.7	20.4
CG	CYSP40/44	POPC	26.1	8.6	42.9	26.5	109.9	+32.2	19.6
CG	CYSP43/44	POPC	26.9	8	36.6	31.1	96.8	+19.1	17.6
CG	CYSP40/43/44	POPC	26.4	8.3	31.2	30.4	103	+25.3	17.2
CG	ASNG66	POPC	26.2	8.5	38.7	26.9	78.6	+0.9	22.5
CG	TMD, no PTM	POPC	25.5	7.7	29.4	31.4	-	-	-
CG	H2+H3, no PTM	POPC	-	-	-	-	82.3	+4.6	26.4
AA	No PTM	POPC	40.2	9.9	48.1	22.6	85.3		49.2
AA	No PTM	Mix	32.6	11.6	50.5	27.2	83.7		32.6

Table S3. Properties of the TM helices in experimentally determined structures of single-helical viroporins.

Protein and virus name	Method	Membrane mimetic	TM residues (length)	Tilt angle	PDB ID	Reference
M2, Influenza A	NMR	DOPC/DOPE	26-46 (21)	32° (N-term) 22° (C-term), pH 7.5	2L0J	[3]
M2, Influenza A	NMR	DMPC	26-46 (21)	30° (N-term) 19° (C-term), pH 7.5	2KQT	[4]
M2, Influenza A	X-ray	OG	25-46 (22)	~35° (N-term), pH 7.3	3BKD	[5]
M2, Influenza A	X-ray	OG	25-46 (22)	16° (pH 7.5-8) 31° (pH 6.5) 38° (pH 3-4)	3LBW	[6]
M2, Influenza B	NMR	POPE, POPC/POPG	6-28 (23)	14° (pH 7.5) 20° (pH 4.5)	6PVR, 6PVT	[7]
Monomeric Vpu, HIV-1	NMR	DMPC	8-25 (18)	25°	2N28	[8]
Vpu, HIV-1	NMR	DOPC/DOPG	8-25 (18)	13°	1PI7, 1PI8	[9]
E, SARS-CoV	NMR	LMPG	8-35 (28)	~24°	5X29	[10]

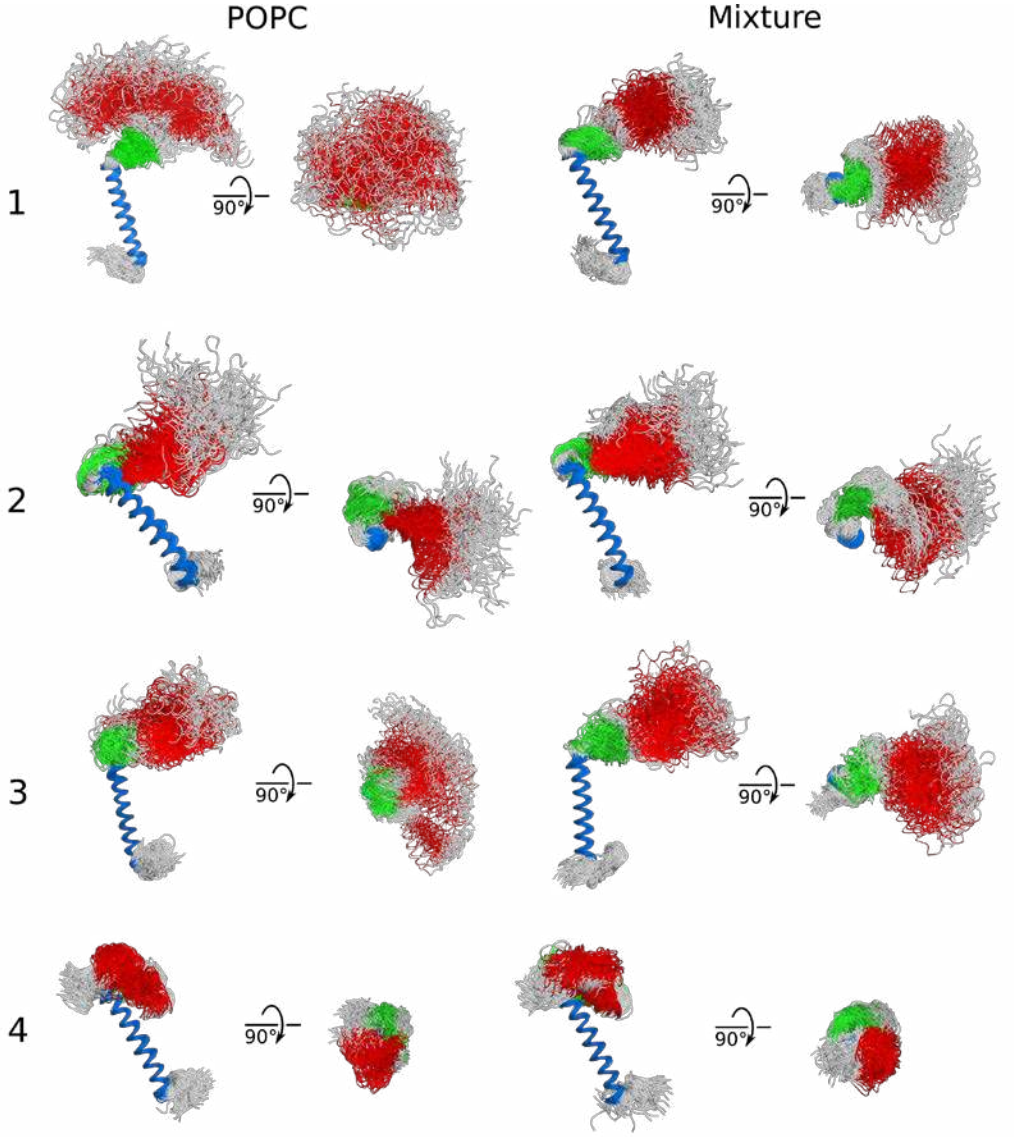

Figure S1. Conformations of the E protein observed in all-atom simulations. Positions of the transmembrane helix were aligned for clarity; helices H2 and H3 are mobile.

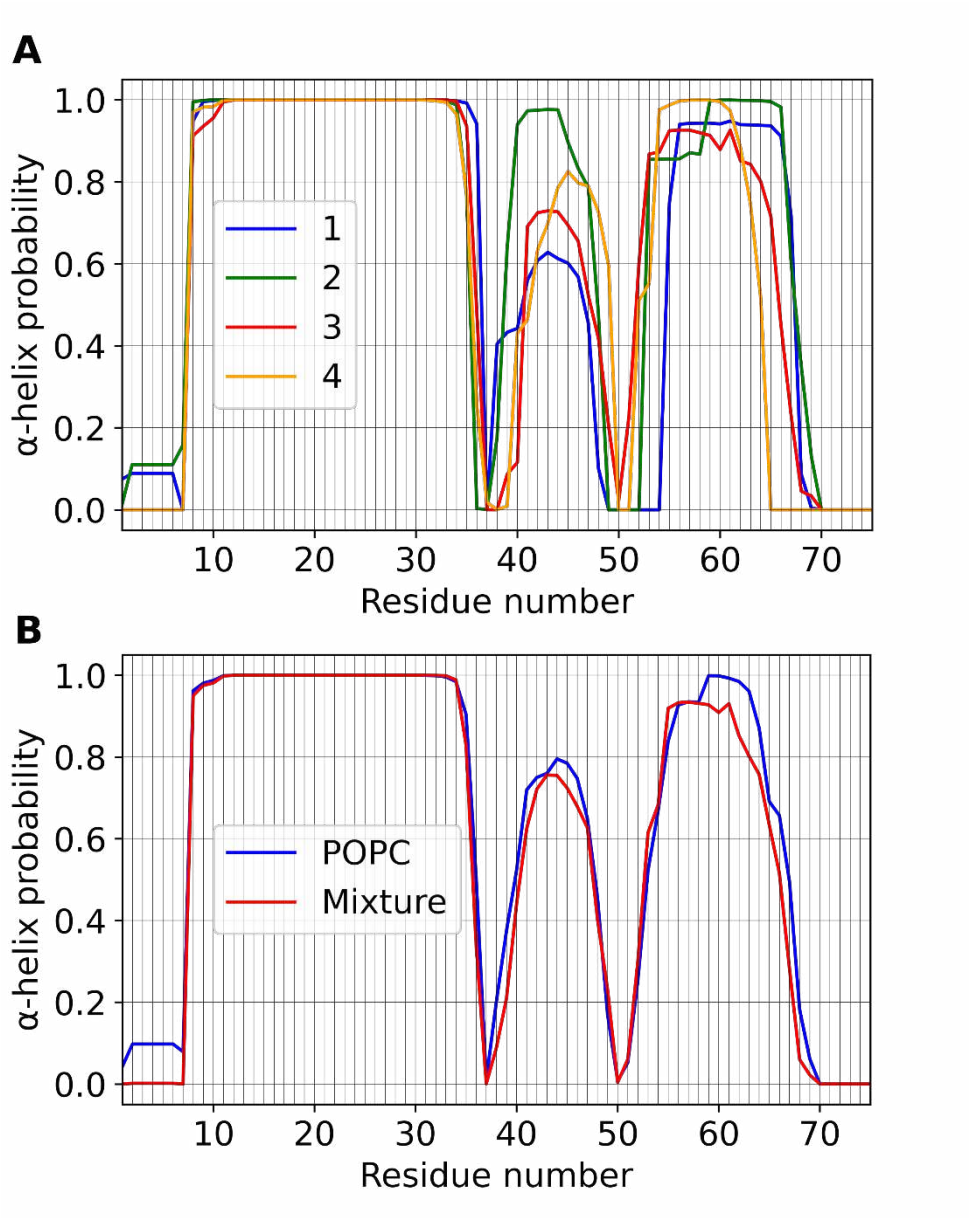

Figure S2. Conservation of the secondary structure of the E protein in AA MD simulations. A) Comparison of secondary structure in simulations with different starting structures (centroids of clusters 1-4). B) Comparison of secondary structure in simulations with the membrane consisting either of POPC or a native-like mixture of lipids. Average probability of observing the α-helical structure for each residue is shown. TMD remains fully α-helical, H2 is sometimes disordered, and H3 is mostly ordered.

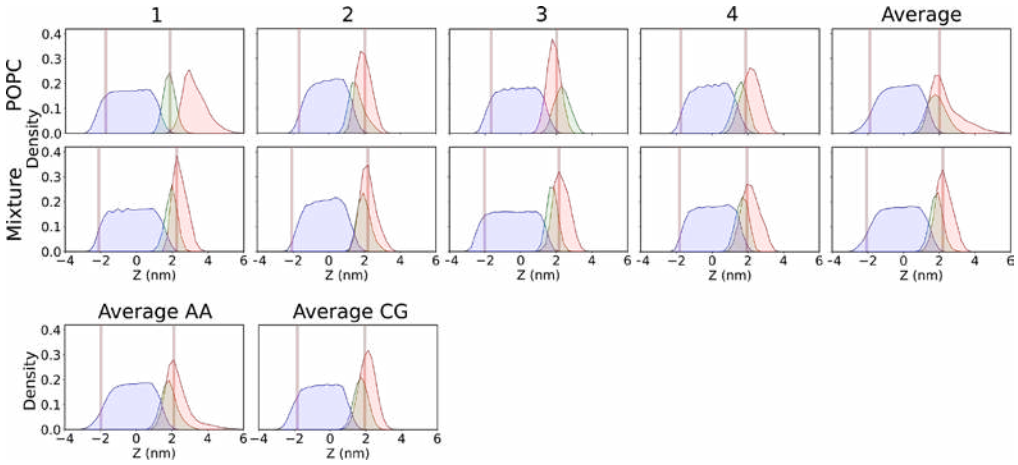

Figure S3. Average positions of TMD, H2 and H3 relative to the membrane in CG and AA simulations of monomeric E protein. Average positions of lipid phosphate groups are shown using brown lines. Distributions of TMD, H2 and H3 backbone atoms' positions are shown in blue, green and red, respectively.

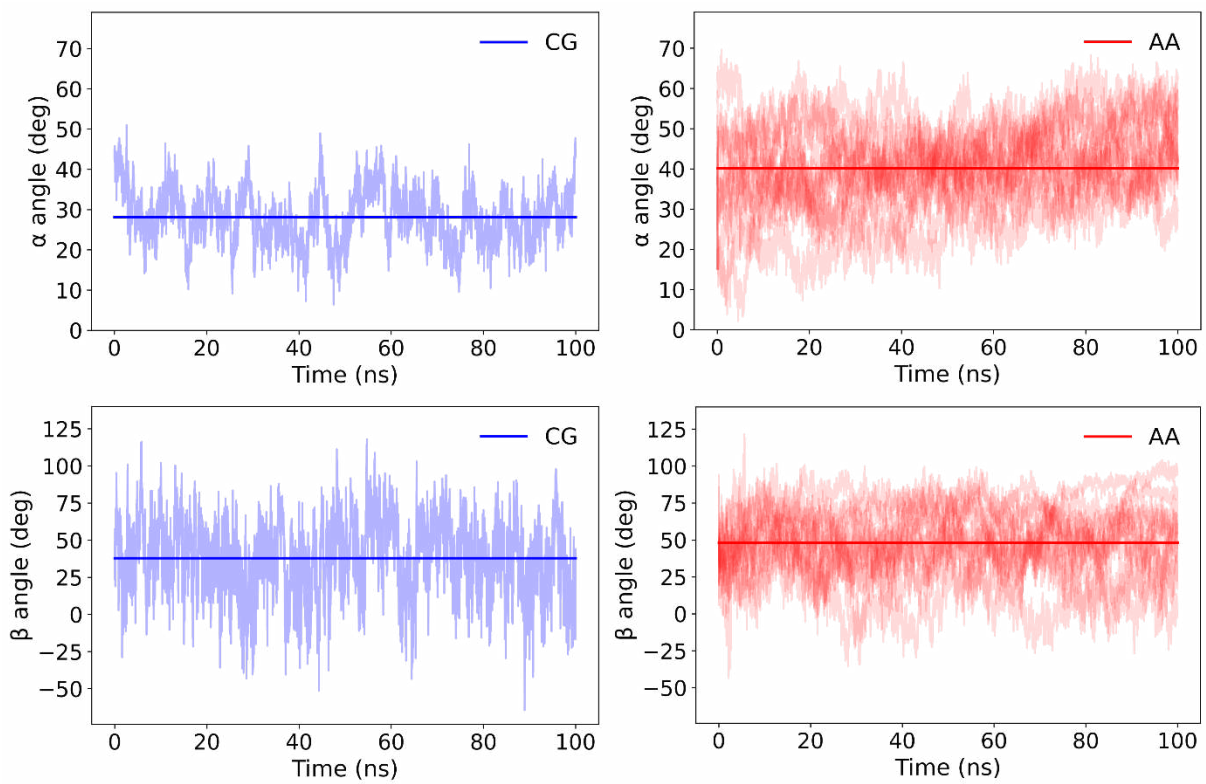

Figure S4. Orientation of TMD in POPC bilayer in coarse-grained (CG, trajectory 1) and all atom (AA, trajectories 13-16) simulations. (top) Distributions of the tilt angles. (bottom) Distributions of the axial rotation angles. Solid lines indicate average values.

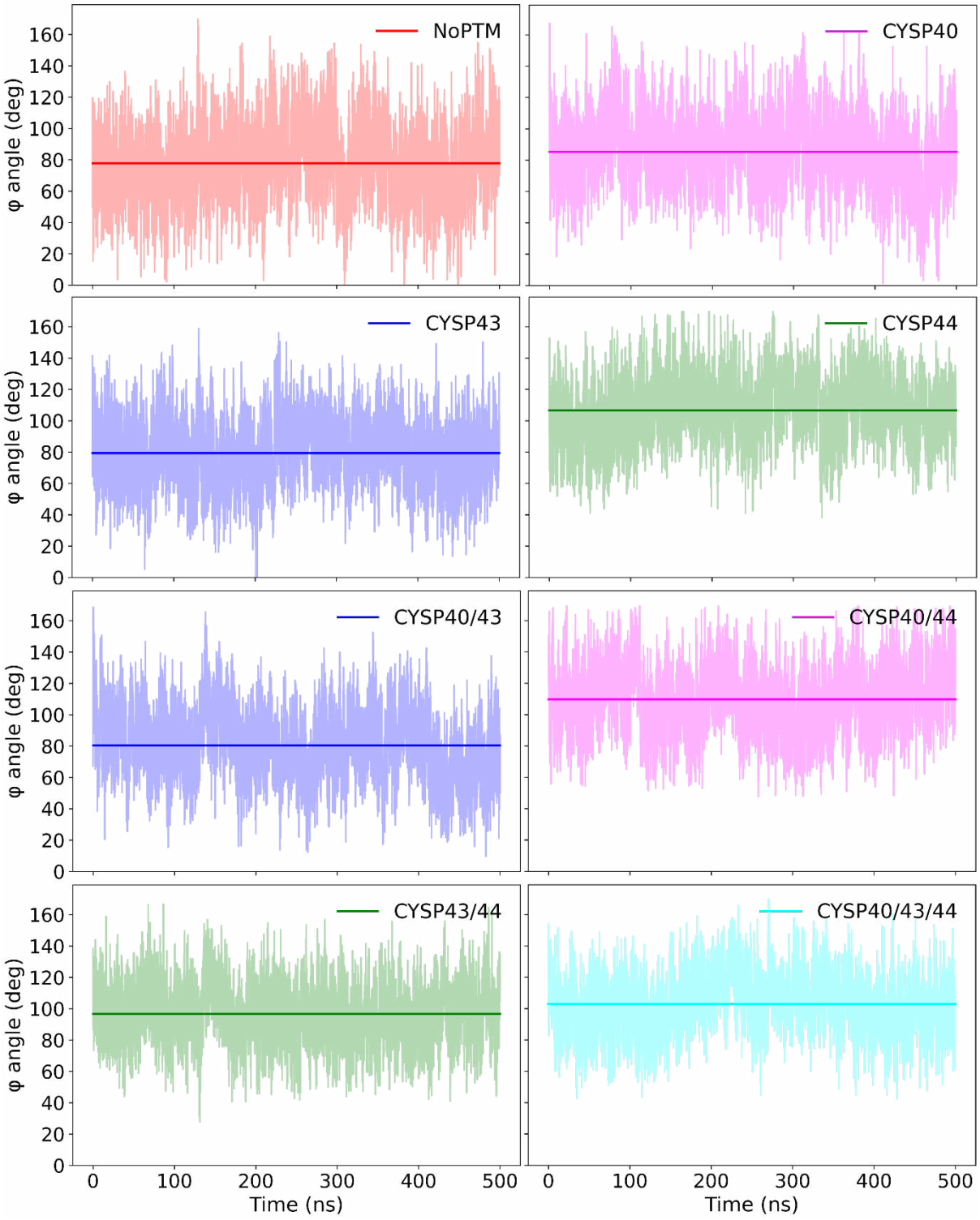

Figure S5. Rotation angles of Cys43 relative to the membrane plane viewed from the N-terminus for trajectories 2-9. Solid lines indicate average values.

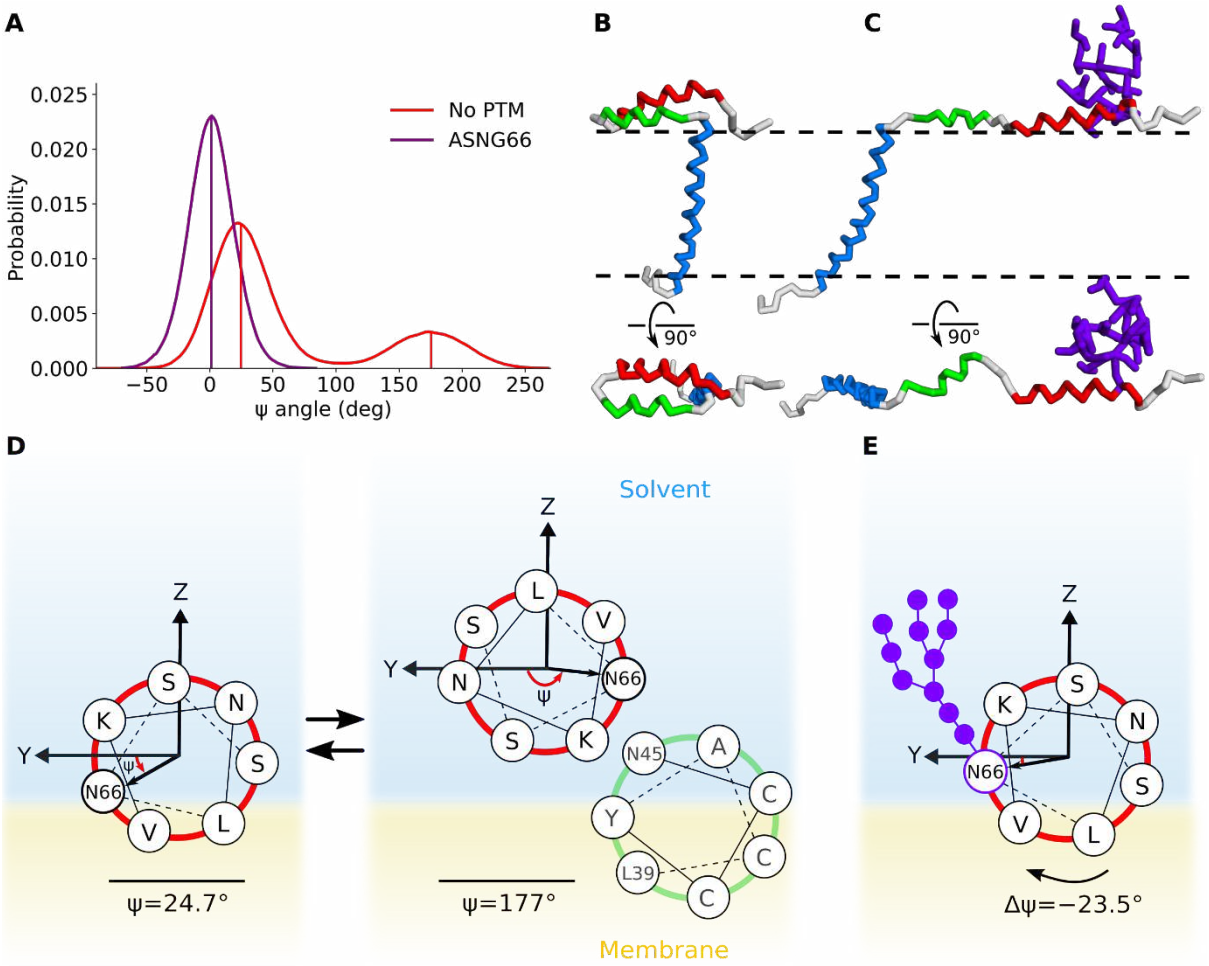

Figure S6. Effect of Asn66 glycosylation on orientation of the helix H3 relative to the membrane in coarse-grained simulations. The glycan moiety is Man9. Rotation of Asn66 relative to the membrane plane (**Y**) viewed from the N-terminus is analyzed. (A) Distributions for the Asn66 rotation angle relative to the membrane plane for unmodified and glycosylated variants. Vertical lines indicate average values. (B) and (C) Representative conformations for $\psi \approx 0°$ and $\psi \approx 180°$. (D) and (E) Schematics showing the H3 orientation with helical wheel projections for unmodified and glycosylated variants. Glycosylation of Asn66 precludes the configuration with $\psi = 177°$.

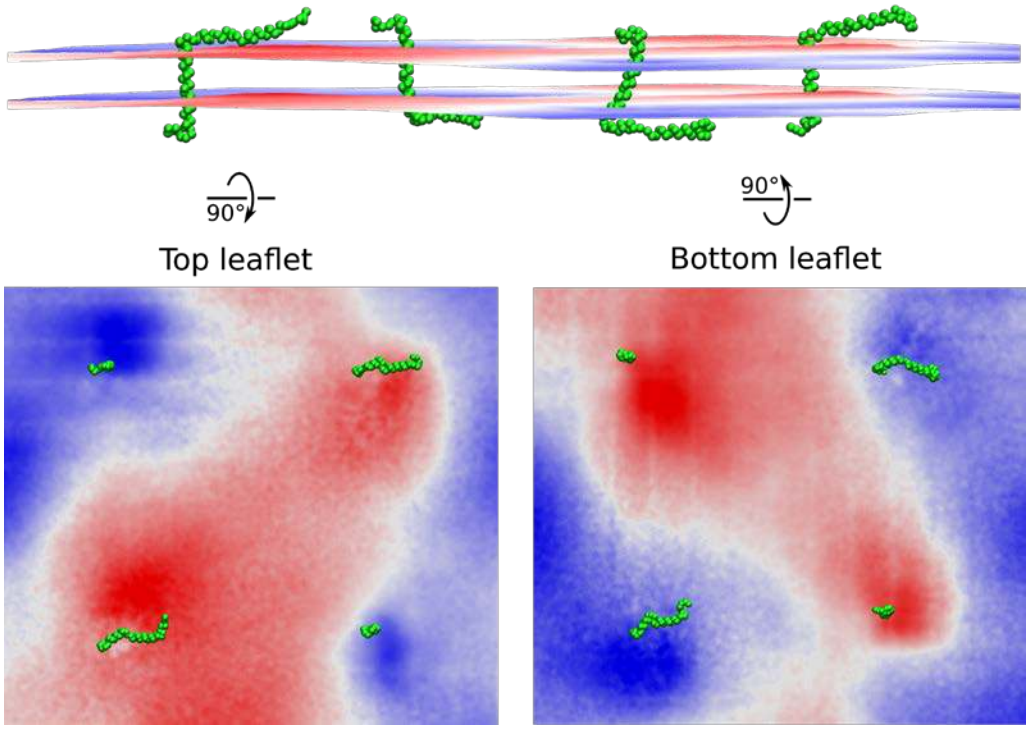

Figure S7. Induction of curvature by the E protein monomers in the system containing 4 proteins. (top) Side view of the simulated system. (left) Top monolayer. (right) Bottom monolayer. Upward displacement of each membrane boundary is shown in red, and downward displacement is shown in blue. Each panel shows an exemplary protein position; positions of the membrane boundaries are averaged over the trajectory length of 1 μs.

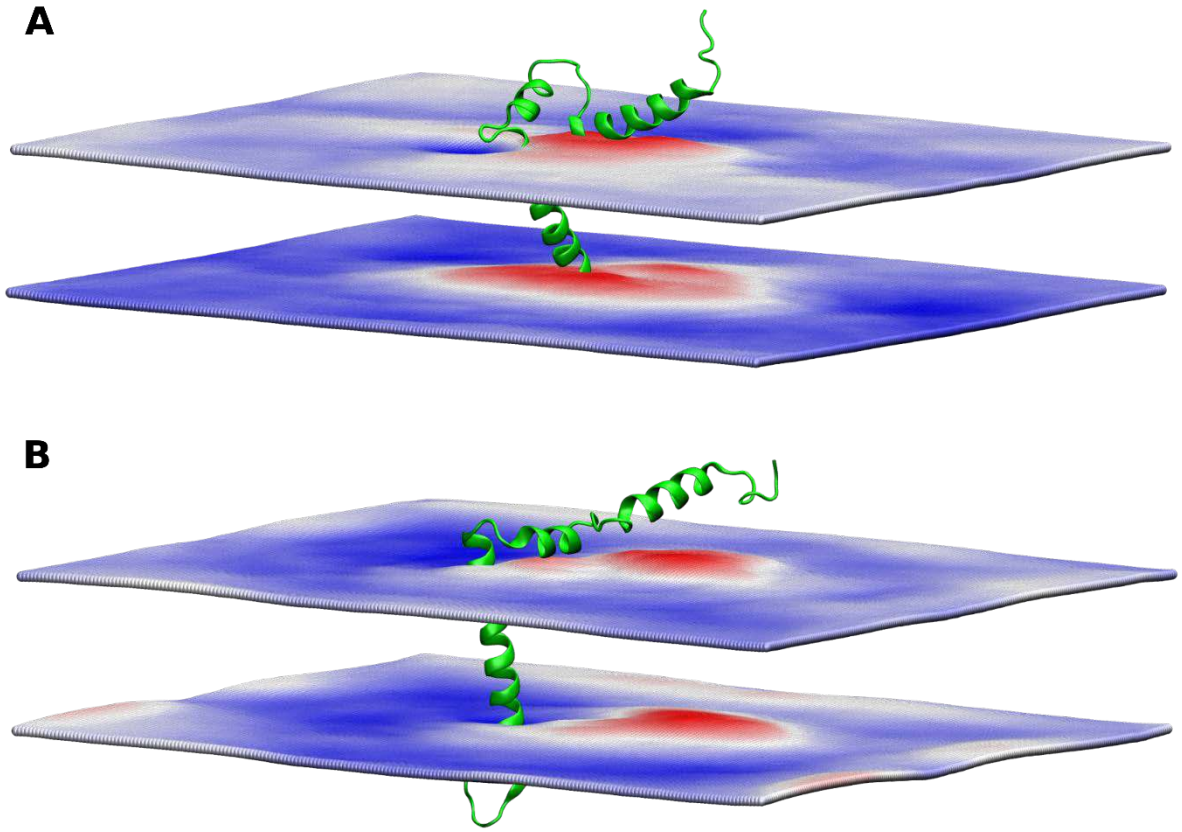

Figure S8. Induction of curvature by the E protein monomer in atomistic simulations. Upward displacement of each membrane boundary is shown in red, and downward displacement is shown in blue. (A) Induction of curvature in the POPC membrane. (B) Induction of curvature in the native-like membrane. The membrane is bent towards the α-helices H2 and H3. Each panel shows an exemplary protein position; positions of the membrane boundaries are averaged over the trajectory length.

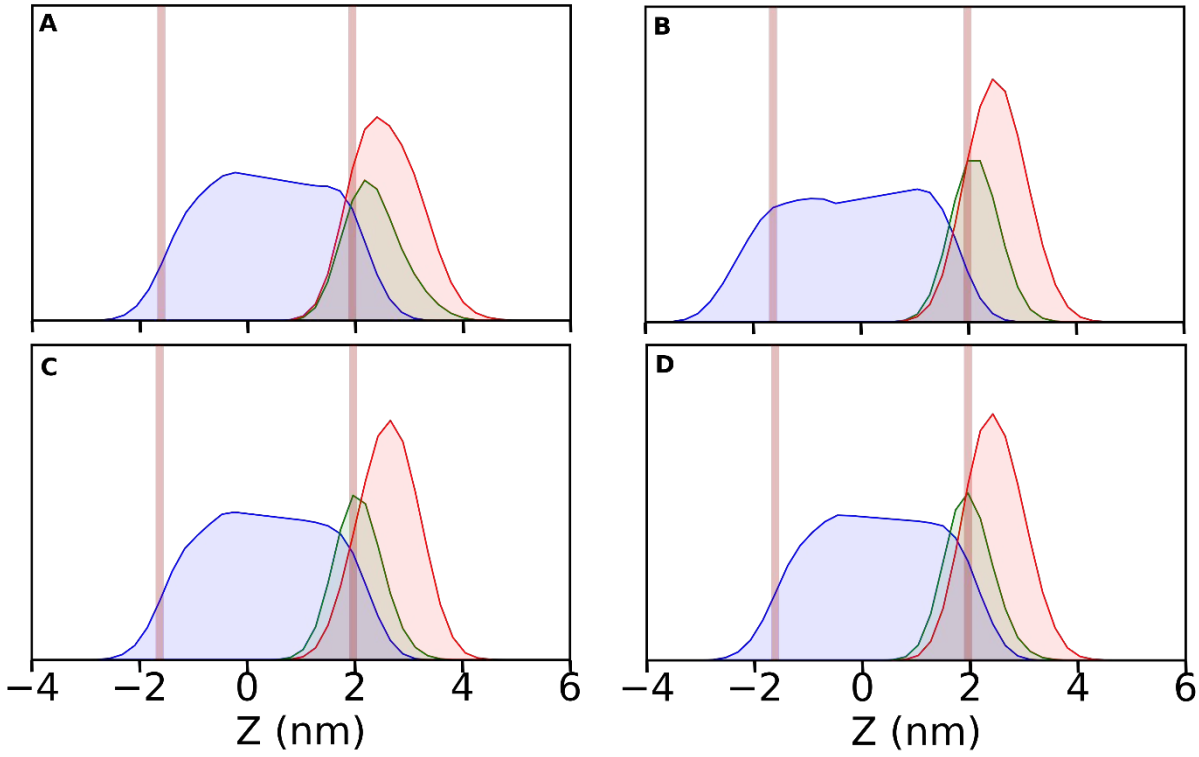

Figure S9. Average positions of TMD, H2 and H3 relative to the membrane in CG simulations of pentameric E protein. (A) Based on the Feig model [11] without PTMs. (B) Based on PDB ID 7K3G [7] for TMD and Feig model [11] for the rest. (C) Based on the Feig model [11] with Cys43 palmitoylated. (D) Based on the Feig model [11] with Cys44 palmitoylated. Average positions of lipid phosphate groups are shown using brown lines. Distributions of TMD, H2 and H3 backbone atoms' positions are shown in blue, green and red, respectively.

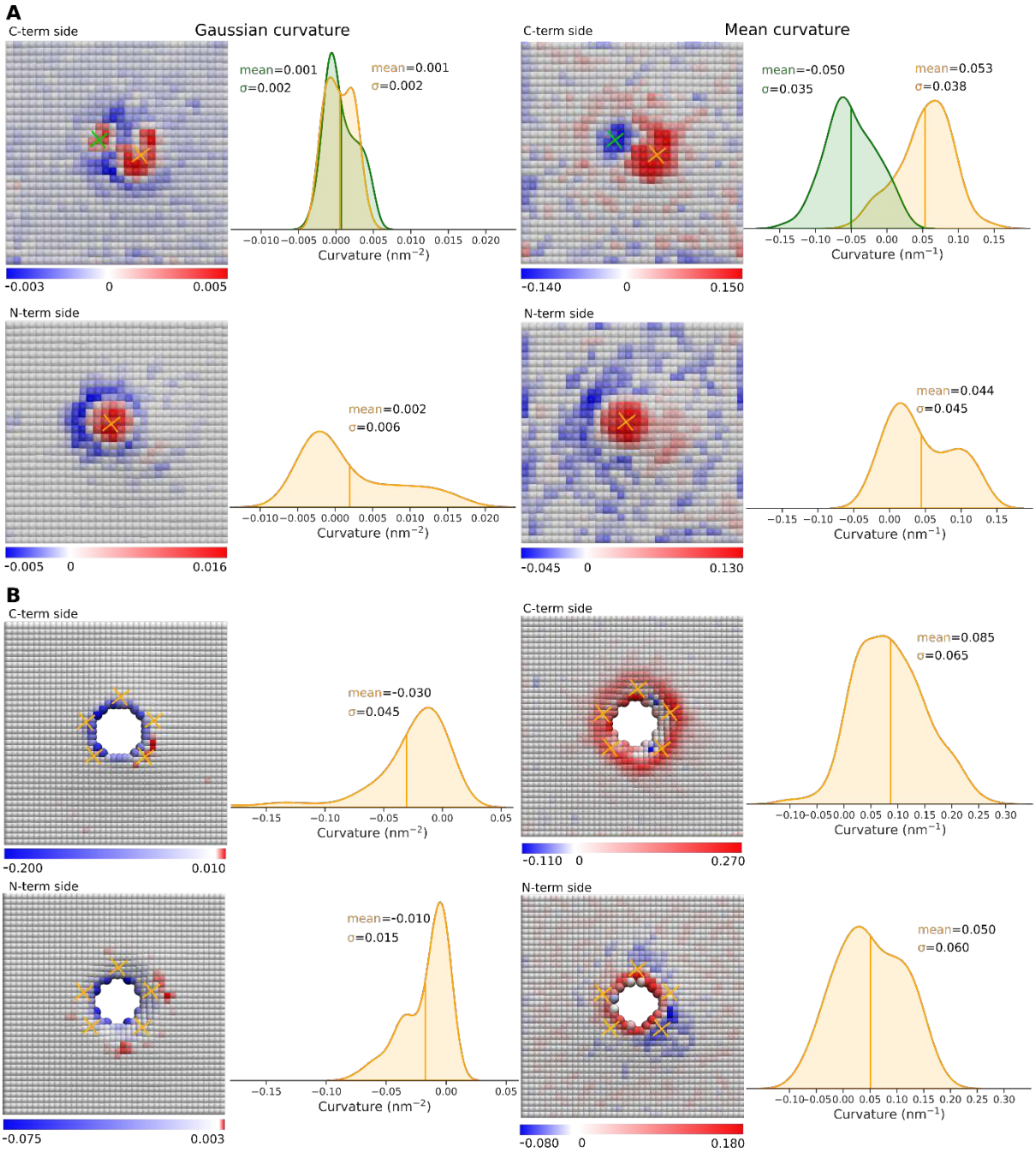

Figure S10. Quantification of curvature induction by the monomeric (A) and pentameric (B) envelope protein. Shown are distributions of Gaussian and Mean curvature in vicinity of the protein (plots inspired by Reference [12]). Protein positions are marked with beige crosses. The systems with the monomeric E protein were aligned prior to the analysis so that the helix H2 always points in the direction of the axis X (to the right in this figure). At the C-terminal side of the membrane with the monomeric E protein, two curved regions are observed, which are marked with the green and beige crosses and are analyzed separately. They approximately correspond to positions of TMD and H2.

SUPPORTING REFERENCES

[1] Q. Yuan, Y. Liao, J. Torres, J.P. Tam, D.X. Liu, Biochemical and functional characterization of the membrane association and membrane permeabilizing activity of the severe acute respiratory syndrome coronavirus envelope protein, Virology. 349 (2006) 264–275. https://doi.org/10.1016/j.virol.2006.01.028.

[2] G. Duart, M.J. García-Murria, B. Grau, J.M. Acosta-Cáceres, L. Martínez-Gil, I. Mingarro, SARS-CoV-2 envelope protein topology in eukaryotic membranes, Open Biology. 10 (2020) 200209. https://doi.org/10.1098/rsob.200209.

[3] M. Sharma, M. Yi, H. Dong, H. Qin, E. Peterson, D.D. Busath, H.-X. Zhou, T.A. Cross, Insight into the Mechanism of the Influenza A Proton Channel from a Structure in a Lipid Bilayer, Science. 330 (2010) 509–512. https://doi.org/10.1126/science.1191750.

[4] S.D. Cady, K. Schmidt-Rohr, J. Wang, C.S. Soto, W.F. DeGrado, M. Hong, Structure of the amantadine binding site of influenza M2 proton channels in lipid bilayers, Nature. 463 (2010) 689–692. https://doi.org/10.1038/nature08722.

[5] A.L. Stouffer, R. Acharya, D. Salom, A.S. Levine, L. Di Costanzo, C.S. Soto, V. Tereshko, V. Nanda, S. Stayrook, W.F. DeGrado, Structural basis for the function and inhibition of an influenza virus proton channel, Nature. 451 (2008) 596–599. https://doi.org/10.1038/nature06528.

[6] R. Acharya, V. Carnevale, G. Fiorin, B.G. Levine, A.L. Polishchuk, V. Balannik, I. Samish, R.A. Lamb, L.H. Pinto, W.F. DeGrado, M.L. Klein, Structure and mechanism of proton transport through the transmembrane tetrameric M2 protein bundle of the influenza A virus, PNAS. 107 (2010) 15075–15080. https://doi.org/10.1073/pnas.1007071107.

[7] V.S. Mandala, A.R. Loftis, A.A. Shcherbakov, B.L. Pentelute, M. Hong, Atomic structures of closed and open influenza B M2 proton channel reveal the conduction mechanism, Nature Structural & Molecular Biology. 27 (2020) 160–167. https://doi.org/10.1038/s41594-019-0371-2.

[8] H. Zhang, E.C. Lin, B.B. Das, Y. Tian, S.J. Opella, Structural determination of virus protein U from HIV-1 by NMR in membrane environments, Biochimica et Biophysica Acta (BBA) - Biomembranes. 1848 (2015) 3007–3018. https://doi.org/10.1016/j.bbamem.2015.09.008.

[9] S.H. Park, A.A. Mrse, A.A. Nevzorov, M.F. Mesleh, M. Oblatt-Montal, M. Montal, S.J. Opella, Three-dimensional Structure of the Channel-forming Trans-membrane Domain of Virus Protein “u” (Vpu) from HIV-1, Journal of Molecular Biology. 333 (2003) 409–424. https://doi.org/10.1016/j.jmb.2003.08.048.

[10] W. Surya, Y. Li, J. Torres, Structural model of the SARS coronavirus E channel in LMPG micelles, Biochimica et Biophysica Acta (BBA) - Biomembranes. 1860 (2018) 1309–1317. https://doi.org/10.1016/j.bbamem.2018.02.017.

[11] L. Heo, M. Feig, Modeling of Severe Acute Respiratory Syndrome Coronavirus 2 (SARS-CoV-2) Proteins by Machine Learning and Physics-Based Refinement, BioRxiv. (2020) 2020.03.25.008904. https://doi.org/10.1101/2020.03.25.008904.

[12] A. Mehregan, S. Pérez-Conesa, Y. Zhuang, A. Elbahnsi, D. Pasini, E. Lindahl, R. Howard, C. Ulens, L. Delemotte, Biophysical characterization of the SARS-CoV-2 E protein, (2021). https://doi.org/10.1101/2021.05.28.446179.